AGU PUBLICATIONS

JGR

Journal of Geophysical Research: Solid Earth

RESEARCH ARTICLE
10.1002/2015JB011917

This article is a companion to *An et al.* [2015] doi:10.1002/2014JB011332.

Key Points:
- High-resolution crust/lithosphere temperature model covering the Antarctic Plate
- A fossil slab of the Phoenix Plate is found beneath the Antarctic Peninsula
- The age-thickness relation of oceanic lithosphere depends on ridge spreading rate

Supporting Information:
- Figures S1–S10

Correspondence to:
M. An,
meijianan@live.com

Citation:
An, M., D. A. Wiens, Y. Zhao, M. Feng, A. Nyblade, M. Kanao, Y. Li, A. Maggi, and J.-J. Lévêque (2015), Temperature, lithosphere-asthenosphere boundary, and heat flux beneath the Antarctic Plate inferred from seismic velocities, *J. Geophys. Res. Solid Earth*, *120*, 8720–8742, doi:10.1002/2015JB011917.

Received 31 JAN 2015
Accepted 1 NOV 2015
Accepted article online 11 NOV 2015
Published online 19 DEC 2015

Temperature, lithosphere-asthenosphere boundary, and heat flux beneath the Antarctic Plate inferred from seismic velocities

Meijian An[1], Douglas A. Wiens[2], Yue Zhao[1], Mei Feng[1], Andrew Nyblade[3], Masaki Kanao[4], Yuansheng Li[5], Alessia Maggi[6], and Jean-Jacques Lévêque[6]

[1]Institute of Geomechanics, Chinese Academy of Geological Sciences, Beijing, China, [2]Department of Earth and Planetary Science, Washington University, St. Louis, Missouri, USA, [3]Department of Geosciences, Pennsylvania State University, University Park, Pennsylvania, USA, [4]National Institute of Polar Research, Tokyo, Japan, [5]Polar Research Institute in China, Shanghai, China, [6]Institut de Physique du Globe de Strasbourg, Université de Strasbourg/EOST, CNRS, Strasbourg, France

Abstract We estimate the upper mantle temperature of the Antarctic Plate based on the thermoelastic properties of mantle minerals and *S* velocities using a new 3-D shear velocity model, AN1-S. Crustal temperatures and surface heat fluxes are then calculated from the upper mantle temperature assuming steady state thermal conduction. The temperature at the top of the asthenosphere beneath the oceanic region and West Antarctica is higher than the dry mantle solidus, indicating the presence of melt. From the temperature values, we generate depth maps of the lithosphere-asthenosphere boundary and the Curie temperature isotherm. The maps show that East Antarctica has a thick lithosphere similar to that of other stable cratons, with the thickest lithosphere (~250 km) between Domes A and C. The thin crust and lithosphere beneath West Antarctica are similar to those of modern subduction-related rift systems in East Asia. A cold region beneath the Antarctic Peninsula is similar in spatial extent to that of a flat-subducted slab beneath the southern Andes, indicating a possible remnant of the Phoenix Plate, which was subducted prior to 10 Ma. The oceanic lithosphere generally thickens with increasing age, and the age-thickness correlation depends on the spreading rate of the ridge that formed the lithosphere. Significant flattening of the age-thickness curves is not observed for the mature oceanic lithosphere of the Antarctic Plate.

1. Introduction

The architecture of the Antarctic Plate (Figure 1) is unique in that it is bordered by six other plates and is almost entirely surrounded by mid-ocean spreading ridges that formed as a result of the breakup of Gondwana in the Late Mesozoic [*Torsvik et al.*, 2010]. Consequently, knowledge of the crustal and upper mantle thermal structure of the Antarctic Plate is essential for understanding the mechanisms responsible for the breakup of Gondwana and the dynamics of global plate motions since the Late Mesozoic [*Sutherland*, 2008; *Torsvik et al.*, 2008].

For most continents, the lithospheric thermal structure is inferred from measurements of surface heat flux, which depends on the geology of the lithosphere and mantle heat flux, and partly controls ice sheet dynamics [*Siegert and Dowdeswell*, 1996; *Fahnestock et al.*, 2001; *Pollard et al.*, 2005; *Llubes et al.*, 2006]. However, the crustal geology and heat flux of Antarctica are difficult to measure due to widespread ice cover. A previous estimate of Antarctic heat flux employed the depth of the Curie temperature isotherm from satellite magnetic data [*Maule et al.*, 2005], although this approach was limited by significant methodological uncertainty and sparse data coverage. The derived heat flux reflected variations in magnetic crustal thickness; however, the magnetic crust beneath regions where the Moho is shallower than the Curie isotherm may have appeared thin due to a lack of magnetic mantle rocks [*Frost and Shive*, 1986; *Wasilewski and Mayhew*, 1992].

Previous studies have shown that temperature is the dominant influence on upper mantle (and even lower mantle) seismic velocity, with composition playing a lesser role [e.g., *Jordan*, 1979; *Nolet and Zielhuis*, 1994; *Sobolev et al.*, 1996; *Goes et al.*, 2000; *Schuberth et al.*, 2009]. Therefore, upper mantle temperatures can be estimated from seismic velocities using a nonlinear inversion and laboratory measurements of the density and elastic moduli of various mantle minerals at high temperatures and pressures [e.g., *Goes et al.*, 2000; *Röhm et al.*, 2000; *Goes and Van der Lee*, 2002; *Cammarano et al.*, 2003; *Shapiro and Ritzwoller*, 2004a;

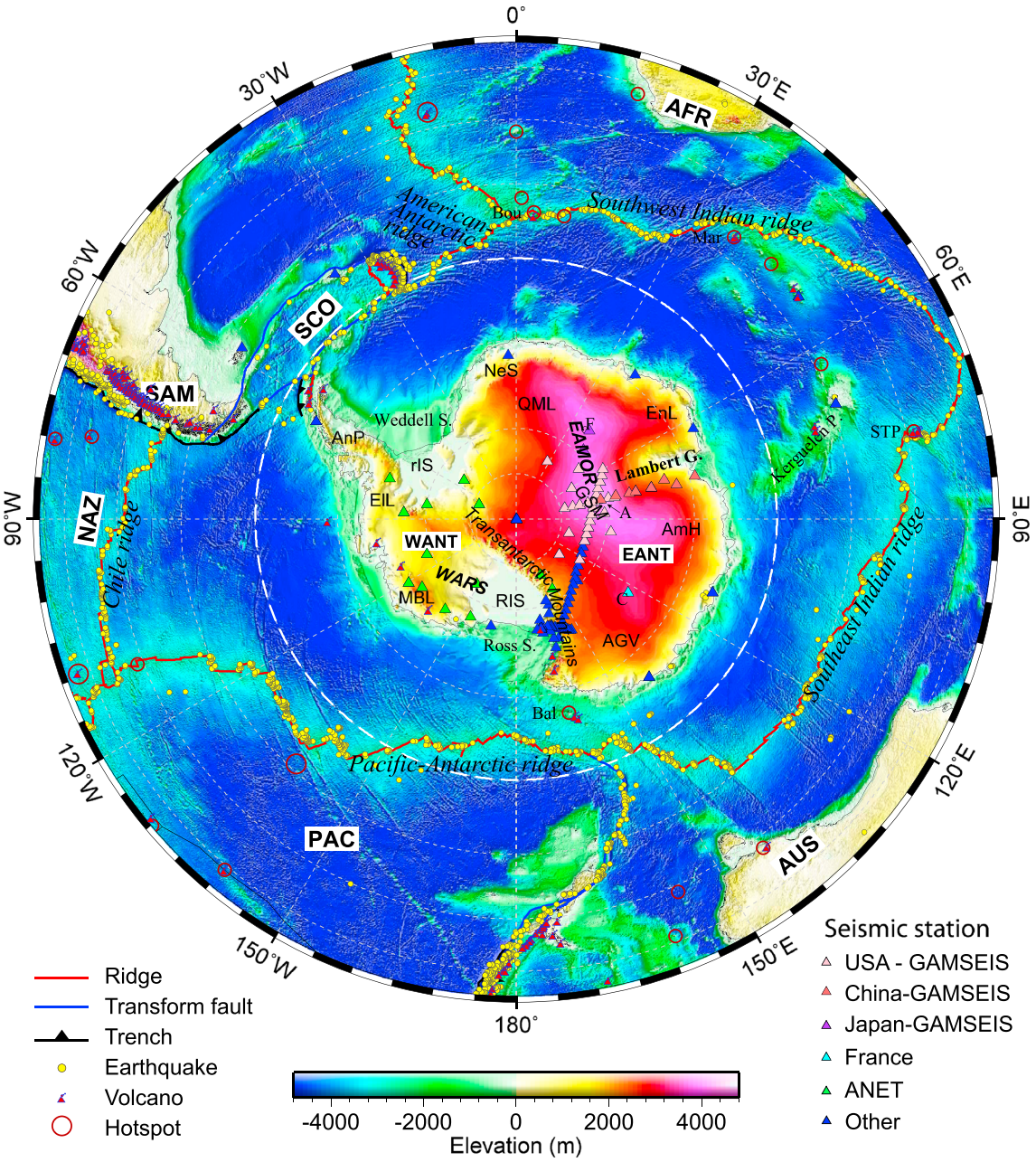

Figure 1. Topographic map of the Antarctic Plate. Data are from the ETOPO2 topography data set. All of the seismic stations and earthquakes indicated in the figure were used to create the AN1-S model of *An et al.* [2015]. A = Dome A (Argus); AFR = African Plate; AIS = Amery Ice Shelf; AmH = American Highland; AUS = Australian Plate; C = Dome C (Circe, Charlie); EAMOR = East Antarctic Mountain ranges; EANT = East Antarctica; EIL = Ellsworth Land; EnL = Enderby Land; F = Dome F (Fuji); GSM = Gamburtsev Subglacial Mountains; MBL = Marie Byrd Land; NAZ = Nazca Plate; NeS = New Schwabenland; PAC = Pacific Plate; QML = Queen Maud Land; rIS = Ronne Ice Shelf; RIS = Ross Ice Shelf; SAM = South American Plate; SCO = Scotia Plate; TAM = Transantarctic Mountains; WANT = West Antarctica; and WARS = West Antarctic rift system. Red circles are proposed hotspots at Foundation [*Ito and van Keken*, 2007], St. Paul Island [*Müller et al.*, 1993], and elsewhere [*Courtillot et al.*, 2003]. Hotspot abbreviations: Bal = Balleny; Bou = Bouvet; Mar = Marion; and STP = St. Paul-Amsterdam. Volcanoes were identified using the Global Volcanism Program of the Smithsonian Institution [*Siebert and Simkin*, 2002].

An and Shi, 2006]. *Shapiro and Ritzwoller* [2004b] derived a low-resolution surface heat flux across Antarctica using seismic velocities from a global seismic model.

Following the Fourth International Polar Year (2007–2008), seismographs were deployed across Antarctica as part of the Gamburtsev Antarctic Mountains Seismic Experiment (GAMSEIS) of the Antarctica's Gamburtsev Province project and the Antarctic Network (ANET) of the Polar Earth Observing Network project.

These instruments have greatly improved station coverage across the entire continent and continue to provide important data for the Antarctic Plate. *An et al.* [2015] used fundamental-mode Rayleigh-wave group velocities from earthquake waveforms, and from Green's functions derived from ambient noise cross correlation between stations, to derive a new 3-D shear wave velocity model (AN1-S) for the Antarctic lithosphere based on single-step surface-wave tomography. That study used data from ~122 broadband seismic stations in Antarctica and surrounding regions, including all GAMSEIS stations and 12 backbone ANET stations, thereby greatly increasing the resolution and spatial coverage compared with continental-scale models prior to 2007.

The primary aim of this study is to extract petrologic or geodynamical information (e.g., temperature and lithospheric thickness) from seismic velocity data. Using the 3-D seismic velocity model AN1-S, we calculate upper mantle temperatures based on the thermoelastic properties of mantle minerals and then estimate crustal temperatures assuming steady state thermal conduction. From this temperature model, we determine the depths to the base of the lithosphere and to the Curie temperature isotherm and surface heat flux across Antarctica.

2. Methods

2.1. Conversion From *S* Velocity to Temperature in the Upper Mantle

We inverted for upper mantle temperature at depths of >50 km or 10 km below the Moho [*An et al.*, 2015] based on the thermoelastic properties of mantle minerals from seismic velocities in the AN1-S model, following *An and Shi* [2006, 2007]. The converted temperature model is AN1-Ts. The method employed here has its origin in the method proposed by *Goes et al.* [2000]. Both anharmonic and anelastic effects [*Minster and Anderson*, 1981; *de Jonge et al.*, 1994] are considered in the forward procedure. In contrast with *Goes et al.* [2000], *An and Shi* [2007] considered iron content in addition to temperature and pressure effects in the forward calculation and used a direct grid search in the nonlinear temperature inversion. *Priestley and McKenzie* [2006, 2013] presented an alternative method for converting *S* velocity to temperature. For the sake of comparison, we also estimated temperatures using their method, i.e., using equations (3) and (5) in *Priestley and McKenzie* [2006] but with a grid search inversion. The results using their methods are similar to the temperatures calculated by *An and Shi* [2006, 2007] at the top of the seismic low-velocity zone (LVZ), but a difference of >200°C is observed at other depths. The supporting information in a later publication [*Priestley and McKenzie*, 2013] shows that the converted temperature can be too low at depths of <150 km beneath old continents or too high beneath young oceanic lithosphere. In contrast, the method proposed by *An and Shi* [2006, 2007] when applied to the same *S* velocities in *Priestley and McKenzie* [2013] does not suffer these limitations. Accordingly, we only discuss the results obtained using the method developed by *An and Shi* [2006, 2007].

The presence of melt and fluid (e.g., water) lowers the seismic velocity of a rock body [*Hirth and Kohlstedt*, 1996; *Karato and Jung*, 1998; *Goes et al.*, 2000]; however, we lack a model that shows the distribution of melt and fluid in the upper mantle beneath the Antarctic Plate. Therefore, we were unable to consider the effects of melt and fluid on the conversion from velocity to temperature; however, we know that the presence of fluid in the mantle may yield overestimated temperatures. Thus, the estimated mantle temperature in this study should be taken as the upper bound, and if the converted temperatures for the upper mantle seem unreasonably high, a possible explanation might be the existence of melt or fluid.

The present study focuses on the Antarctic Plate, which comprises a range of tectonic elements including cratons, rifts, and oceans that each has a distinct upper mantle composition [*Dick et al.*, 1984; *McDonough and Rudnick*, 1998]. It would be reasonable to consider 3-D compositional heterogeneities in the temperature conversion, as done in forward calculations by *Fullea et al.* [2009]; however, the effect of composition generally yields velocity anomalies that are <1% in the shallow mantle, meaning the compositional effects are difficult to resolve from seismic tomography [*Goes et al.*, 2000; *Schutt and Lesher*, 2006]. A uniform noncratonic mantle composition (olivine 68%, orthopyroxene 18%, clinopyroxene 11%, garnet 3%, and iron content 0.1) [*Dick et al.*, 1984; *McDonough and Rudnick*, 1998; *Shapiro and Ritzwoller*, 2004a] is used for the entire study region. Forward calculations [*An and Shi*, 2006] show that cratonic and oceanic compositions can increase the estimated temperatures by 15–120°C and 5–50°C, respectively, compared with a noncratonic composition.

At high temperatures, anelasticity has a strong effect on seismic velocity [*Karato*, 1993]. A strongly temperature-dependent anelasticity model [*Berckhemer et al.*, 1982; *Kampfmann and Berckhemer*, 1985] yields temperature estimates that are 0–180°C lower than those obtained using the model [*Sobolev et al.*, 1996; *Goes et al.*, 2000] used here. In addition, uncertainties in the *S* velocity model result in temperature uncertainties; e.g., an *S* velocity variation of 0.1 km/s can cause a 50–250°C temperature variation. The combined effects of various factors on temperature uncertainty may be additive or subtractive, making it difficult to quantify the uncertainty in our temperature model, which may vary from tens to several hundreds of degrees centigrade [*Feng et al.*, 2010]. As in previous studies [*Goes et al.*, 2000; *An and Shi*, 2006, 2007], a temperature uncertainty of ~150°C is assumed in the present conversion.

2.2. Crustal Temperatures and Heat Flux Calculations

Because crustal thickness (<60 km) is smaller than the lateral extent of cells (~120 km) used in the tomography of *An et al.* [2015], lateral thermal conduction in the crust can be ignored. Therefore, we estimate the crustal temperatures for each cell by solving a 1-D steady state heat conduction equation with the boundary conditions of a bedrock surface temperature of 0°C and with upper mantle temperature estimated from seismic velocities, as discussed above. The steady state thermal conduction equation is as follows:

$$\nabla \cdot k \nabla T = -A, \tag{1}$$

where A and k are heat productivity (μWm^{-3}) and conductivity ($Wm^{-1}K^{-1}$), respectively. Steady state thermal calculations, as done here, may be invalid if the heat flux exceeds ~90 mWm^{-2}, and higher values indicate melting in the crust or a weak lithospheric mantle [*Jaupart and Mareschal*, 2007]. Such calculations may also be invalid due to tectonic processes such as subduction or subduction termination that have occurred beneath the Antarctic Peninsula.

We first divide the crust of each cell equally into upper, middle, and lower crust using the crustal thickness proposed by *An et al.* [2015]. Since the most common upper crustal minerals have a heat production of ~1 μWm^{-3} [*Rudnick and Fountain*, 1995; *Hasterok and Chapman*, 2011], the heat productivity for the upper crust is set to 1 μWm^{-3}. The heat productivities for the middle crust, lower crust, and upper mantle are respectively set at 0.4 [*Pinet and Jaupart*, 1987], 0.1, and 0.01 μWm^{-3} [*Artemieva and Mooney*, 2001]. We use constant conductivities of 2.25, 2.0 [*Artemieva and Mooney*, 2001], and 4.0 $Wm^{-1}K^{-1}$ [*Schatz and Simmons*, 1972] for the middle crust, lower crust, and upper mantle, respectively. Laboratory measurements show that conductivity depends inversely on temperature for minerals of the crust (1.5–4.0 $Wm^{-1}K^{-1}$) [*Clauser and Huenges*, 1995; *Whittington et al.*, 2009] and upper mantle (olivine, wadsleyite, and ringwoodite) (2−5 $Wm^{-1}K^{-1}$) [*Schatz and Simmons*, 1972; *Xu et al.*, 2004; *McKenzie et al.*, 2005]. This correlation indicates that the strongest dependence on temperature occurs in the upper crust where Earth's interior temperature is lowest; therefore, upper crust conductivity ($Wm^{-1}K^{-1}$) is estimated from a relationship with temperature (T, °C) [*Cermak*, 1982; *Artemieva and Mooney*, 2001]: $k = 3.0/(1 + 0.001\,T)$. To distinguish from temperatures converted directly from seismic velocities (AN1-Ts), the temperatures calculated using the steady state thermal conduction equation are labeled AN1-Tc. In calculating crustal temperatures, we also obtained the surface heat flux in Antarctica.

The above thermal parameters are from general studies on continental minerals and are applied uniformly across the entire plate but may be not suitable for specific tectonic regions. However, because the temperatures at the bedrock surface and uppermost upper mantle are fixed, changes in the thermal parameters do not significantly affect the results. For example, the calculated heat production may be higher than the actual heat production of oceanic crust; however, because the oceanic crust is thin and the temperatures at the surface and uppermost mantle are constrained, the errors in the calculated temperatures caused by uncertainties in the thermal parameters are mostly <1°C.

3. Results

The lithospheric temperature model (AN1-T) of the Antarctic Plate was constructed by combining the upper mantle temperatures (T_s) of AN1-Ts converted from the *S* velocity model AN1-S [*An et al.*, 2015] and the steady state thermal conductive temperatures (T_c) of AN1-Tc calculated using the boundary conditions from AN1-Ts. The resolution lengths in the AN1-T model are therefore similar to those of AN1-S. The resolution

length along a meridian is larger than that along a line of latitude, particularly for an oceanic region, given that most of the observation stations are located within continental Antarctica and that the earthquakes occur at the surrounding plate boundaries (Figure 1). The horizontal resolution length of the *S* velocity model increases with depth, i.e., ~120 km in the crust beneath Antarctica, ~500 km at a depth of 120 km, and ~750 km at a depth of 200 km. The vertical resolution length also increases with depth. For example, beneath the Gamburtsev Subglacial Mountains the vertical resolution lengths are ~10 km down to 60 km, ~25 km down to 150 km, and ~50 km down to 250 km. The vertical resolution length for a discontinuity in a velocity model should be smaller than the vertical resolution in the velocity model [*An*, 2012]. So the vertical resolution length for the lithosphere-asthenosphere boundary (LAB) in the present case should be smaller than 25–50 km, as the LAB occurs mainly at depths of ~100−250 km.

In the temperature model AN1-T, depths refer to the distance beneath the ice surface, and thicknesses are also measured from the ice surface. The thermal boundary layer of a convecting mantle is often referred to as the thermal lithosphere, and it can support large stresses over a long period of time. The upper boundary of fully convecting mantle (i.e., the shallowest depth with an adiabat of the mantle potential temperature) is usually taken to coincide with the LAB, the base of the thermal lithosphere [*Rudnick et al.*, 1998; *Jaupart and Mareschal*, 1999; *Artemieva and Mooney*, 2001; *An and Shi*, 2006]. Here we use the shallowest position with a temperature crossing the 1330°C adiabat as the thermal LAB position.

3.1. 3-D Thermal Models

3.1.1. Representative 1-D Profiles

Figure 2 shows three examples of 1-D *S* velocity and converted temperature profiles, representative of regions beneath East Antarctica (Figure 2a), West Antarctica (Figure 2b), and oceanic parts of the Antarctic Plate (Figure 2c).

Beneath the Gamburtsev Subglacial Mountains, which mark a cratonic suture in East Antarctica [*An et al.*, 2015], upper mantle temperatures (Figure 2a) increase downward and first cross the 1330°C adiabat at a depth of ~225 km, which is considered the lithospheric base or LAB. Below this depth, the *S* velocities decrease, indicating that the top of the seismic low-velocity zone (LVZ) is close to the thermal LAB. This correspondence between the seismic and thermal LAB has been noted in a previous study of the temperature of continental lithosphere in China [*An and Shi*, 2006] using *S* velocities from *Huang et al.* [2003]. We calculate a surface heat flux of 47 mWm^{-2} for the Gamburtsev profile.

Beneath the West Antarctic rift system (Figure 2b), the thermal LAB is at ~90–100 km depth, and the uppermost seismic LVZ (seismic asthenosphere) is at ~100 km depth. Notably, the temperatures at depths of 100–150 km are equal to or higher than the dry mantle solidus. Immediately below, at depths of 150–200 km, temperatures are 100°C lower than those in the overlying thermal layer. We calculate a surface heat flux of 68 mWm^{-2} for the West Antarctica profile.

Temperatures beneath a position of the southernmost Southern Pacific Ocean (Figure 2c), which is representative of regions underlain by thin (<10 km) oceanic crust, indicate that the LAB occurs at a depth of ~70–80 km, close to the top of the seismic LVZ. As with the West Antarctic mantle (Figure 2b), temperatures in the oceanic profile are higher than the dry mantle solidus, indicating that a hydrous or partial melt may exist in the asthenosphere. We calculate a surface heat flux of 58 mWm^{-2} for the oceanic profile (Figure 2c).

3.1.2. Representative Horizontal Slices

Temperature maps converted from seismic velocity for the upper mantle at depths of 100 and 150 km are shown in Figure 3, and steady state conduction temperature maps for depths of 10 and 20 km are shown in Figure 4. Because depth and *S* velocity are the two primary parameters in the conversion from *S* velocity to temperature in the upper mantle, the anomaly patterns of seismic-thermal temperatures at a given depth should be similar to those of *S* velocities [*An et al.*, 2015] at that depth.

At 100 km depth (Figure 3a), the temperatures beneath East Antarctica are lower than the assumed mantle adiabat of 1330°C, whereas the temperatures beneath West Antarctica and most of the oceanic regions are close to or higher than 1330°C. Of note is the oceanic region between 20°E and 100°E, which is composed of old crust (~100 Ma; Figure S1a in the supporting information) and includes low temperatures similar to those beneath the neighboring continental East Antarctica. High-temperature regions occur beneath some hotspots (e.g., the Balleny and Marion hotspots) and most volcanoes. These high-temperature anomalies

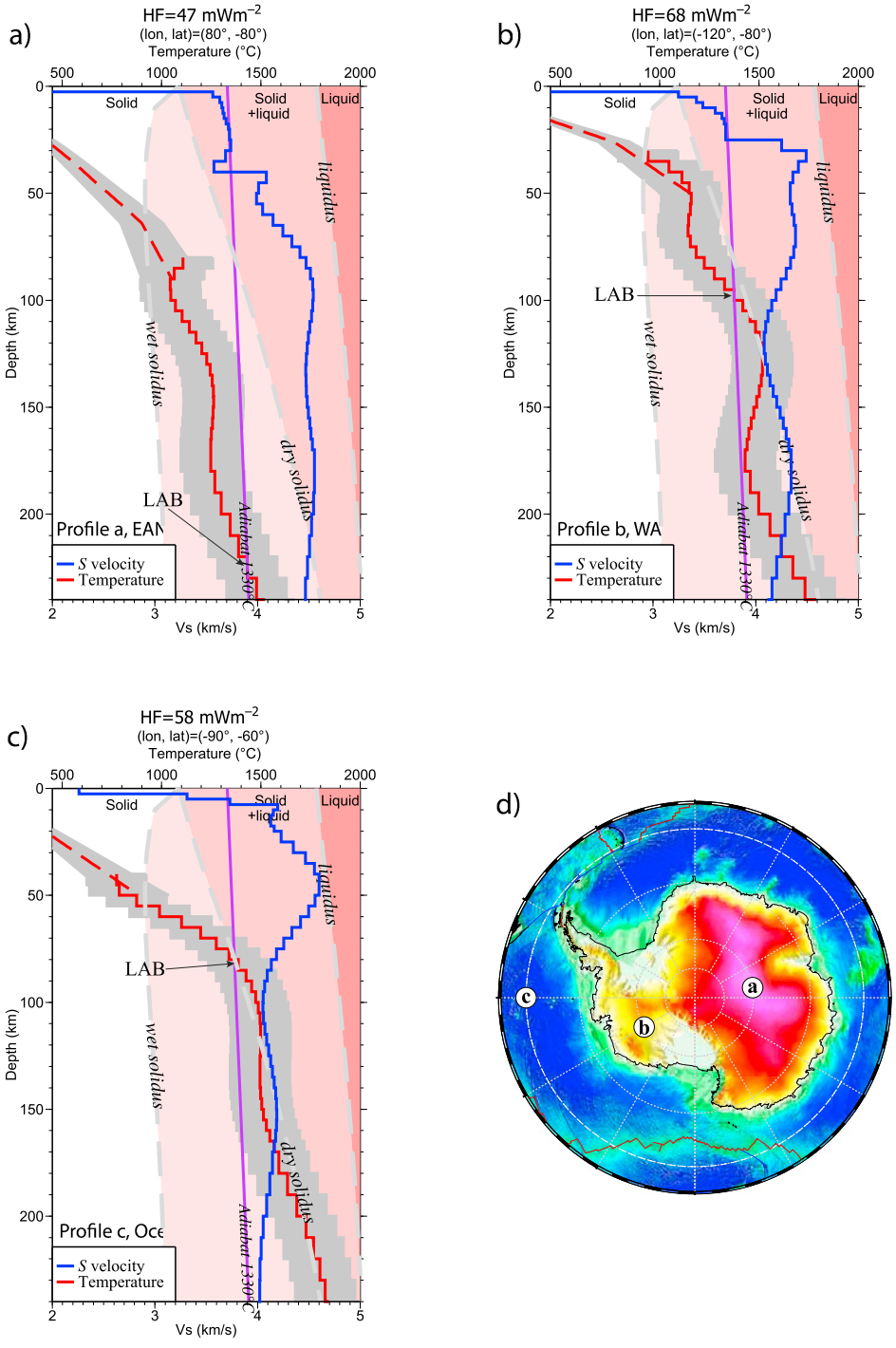

Figure 2. Representative 1-D temperature profiles for (a) East Antarctica (EANT), (b) West Antarctica (WANT), and (c) oceanic regions. (d) Profile locations. The age of the oceanic crust at "c" is ~60 Ma. The *S* velocities are the same as those in Figure 5 of *An et al.* [2015]. Red solid and red dash lines are seismic-thermal temperatures from AN1-Ts with ± 150°C uncertainties (gray area) and steady state temperatures from AN1-Tc with uncertainties (gray area), respectively. The water-saturated (wet) and dry mantle solidi (gray thick dashes) and liquidus are from *Katz et al.* [2003]. The adiabat of a potential temperature of 1330°C was calculated using a mantle adiabatic gradient of 0.45°C/km [*Katsura et al.*, 2010]. HF is the estimated heat flux.

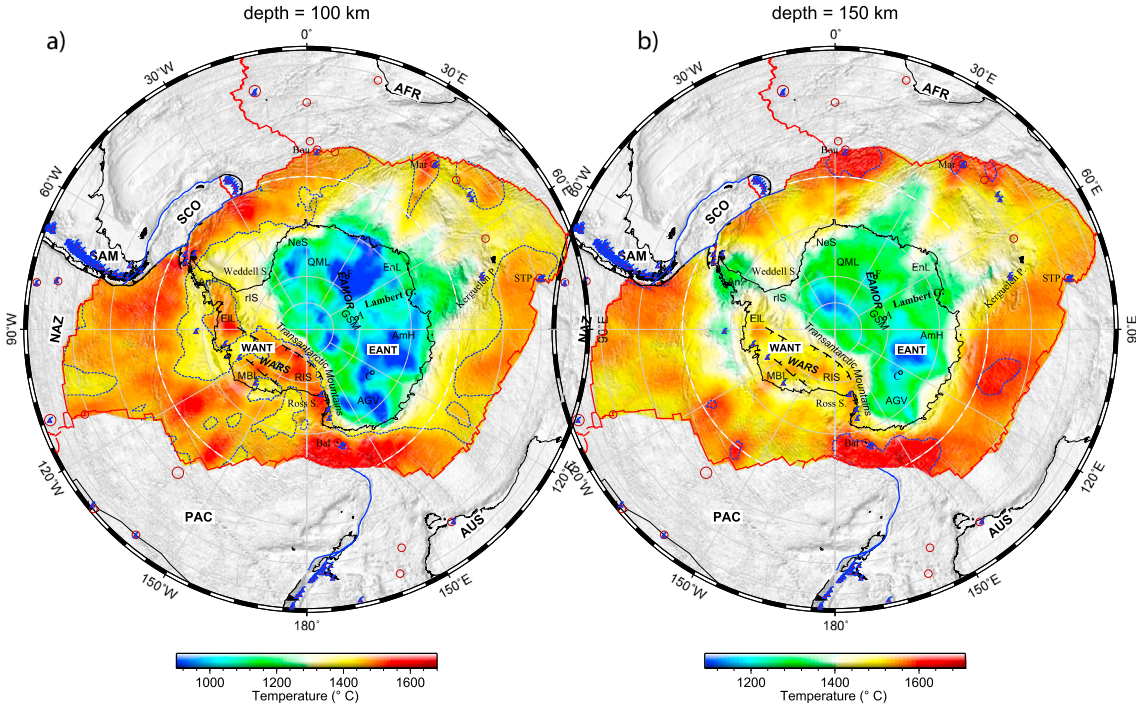

Figure 3. Seismic-thermal temperature (AN1-Ts) maps at depths of (a) 100 km and (b) 150 km. Blue dashes indicate the isocontour of the dry mantle solidus at each depth. Symbols are as in Figure 1.

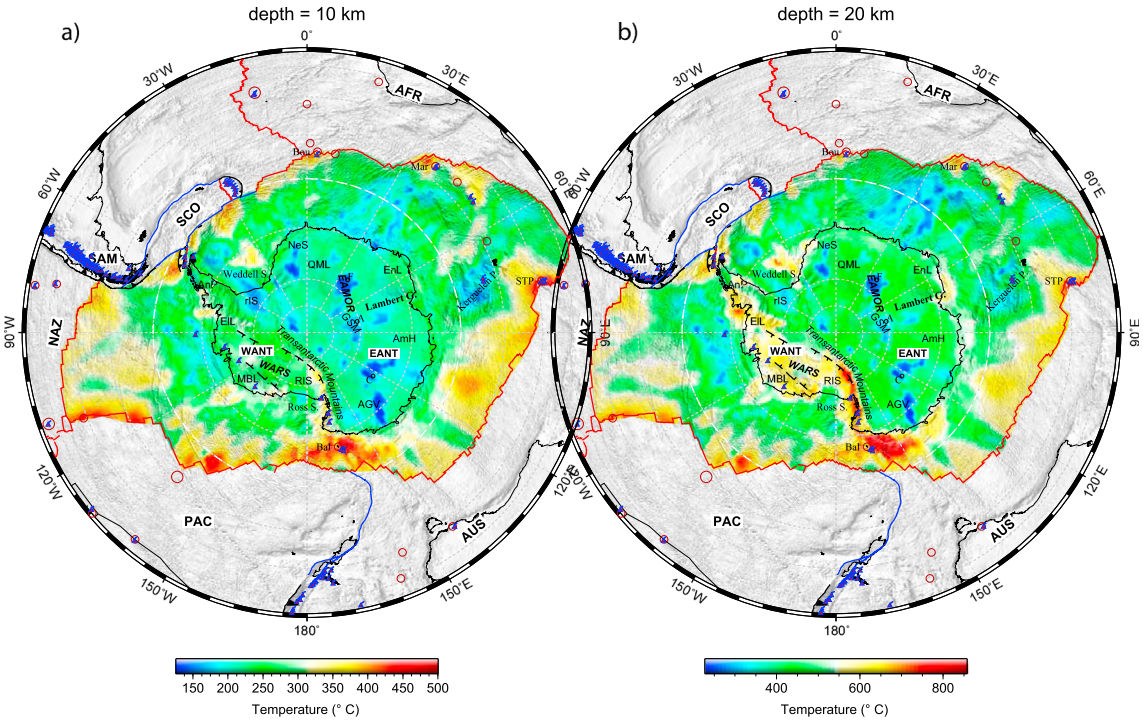

Figure 4. Conductive temperature (AN1-Tc) maps at depths of (a) 10 km and (b) 20 km. Symbols are as in Figure 1.

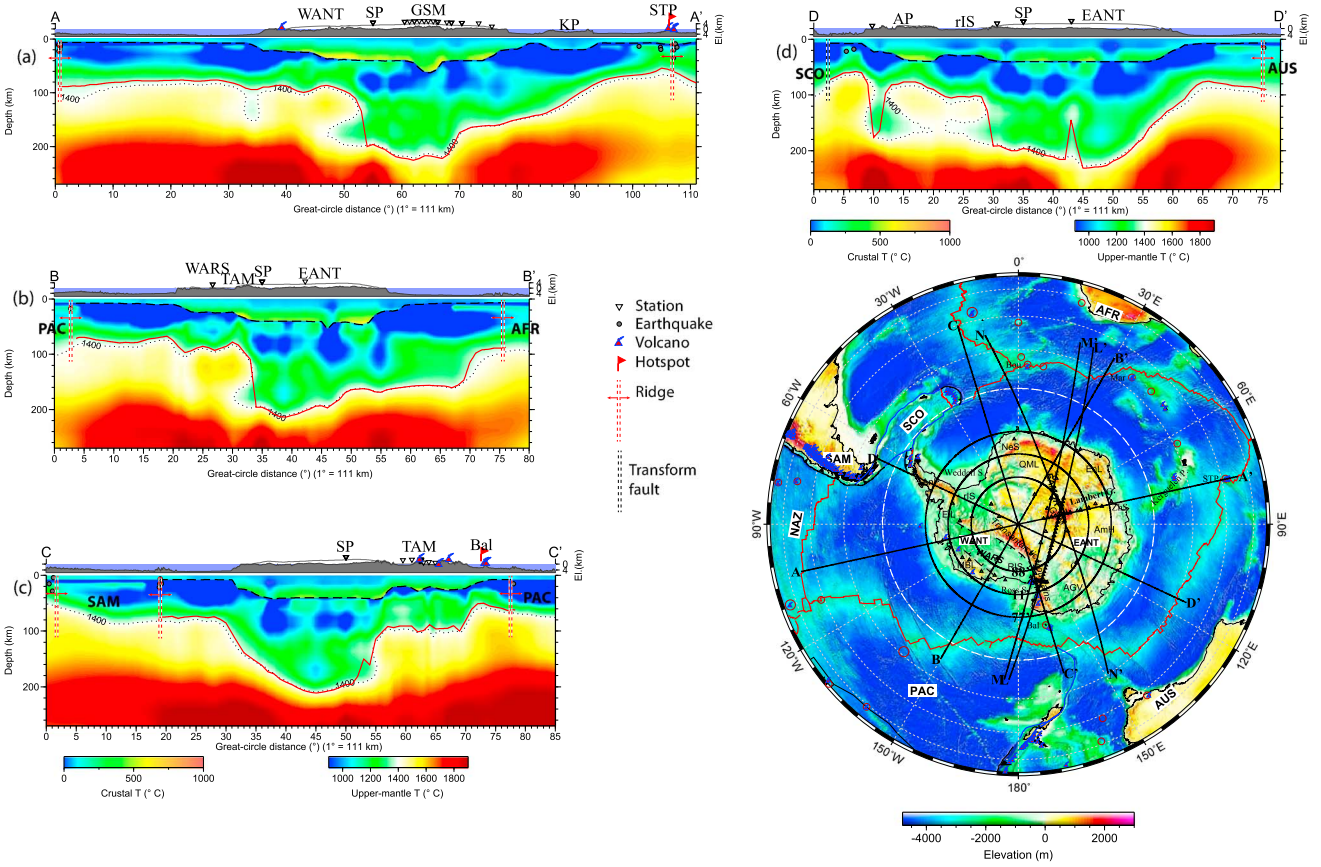

Figure 5. Representative vertical temperature transects. The mantle temperature (right-hand color scale) was converted from the seismic velocity, and the crustal temperature (left-hand color scale) was calculated from steady state thermal conduction. Transect locations are the same as those for the velocity transects in *An et al.* [2015] and are shown in the inset plot, where the shaded bedrock surface is from Bedmap2 [*Fretwell et al.*, 2013], and other surface topography is from ETOPO2. The transects in (a–d) cross the South Pole, in (e–g) cross the GAMSEIS array, and in (h–j) are along the latitudes of 70°S, 75°S, and 80°S, respectively. The transects are as follows: In Figure 5a A-A′ crosses the South Pole, the Gamburtsev Subglacial Mountains (GSM), and the St. Paul-Amsterdam hotspot (STP); Figure 5b B-B′ crosses West Antarctica, the South Pole, and East Antarctica; Figures 5e L-L′ and 5f M-M′ cross the Transantarctic Mountains (TAM) and GSM; Figure 5g N-N′ crosses Domes A and C. The black and gray shaded areas indicate exaggerated continental and oceanic topography, respectively. Open inverted triangles indicate seismic stations used in the inversion for AN1-S. Red flags mark hotspot sites [*Müller et al.*, 1993; *Courtillot et al.*, 2003; *Ito and van Keken*, 2007], and red-filled triangles indicate volcanoes, the positions of which are from the Global Volcanism Program, Smithsonian Institution [*Siebert and Simkin*, 2002]. Thick black dashes marking the Moho are from *An et al.* [2015]. Black dots are the isothermal contour for 1400°C. Red lines indicate the thermal lithospheric base or the lithosphere-asthenosphere boundary (LAB). Red dashes with two arrows mark mid-ocean ridges. KP = Kerguelen Plateau; SP = South Pole.

extend to depths of 150 km (Figure 3b) and 200 km (not shown here). The temperatures beneath some oceanic regions and West Antarctica (Figure 3a) are so high as to be above the dry mantle solidus, indicating that hydrous or partial melt exists in those regions at a depth of 100 km.

The distribution of anomalies at a depth of 150 km (Figure 3b) is generally similar to that at 100 km depth in the eastern Antarctic Plate (0°–180°E). In contrast, differences between the two depths are apparent in the oceanic region off the coast of West Antarctica (0°–180°W). In this region, which contains oceanic crust older than 50 Ma (supporting information Figure S1a), temperatures are lower than in regions of younger oceanic crust and even lower than in the region of the continental West Antarctic rift system. Areas with temperatures higher than the dry mantle solidus at 150 km depth (Figure 3b) are much smaller than those at 100 km depth (Figure 3a). Two areas in East Antarctica (Figure 3b) have temperatures lower than 1200°C, indicating deep lithospheric roots. A low-temperature region exists beneath the Antarctic Peninsula at 150 km depth. Higher temperatures at shallower depths in this region preclude a thick lithosphere but may indicate a stalled subducted slab (see section 4.3).

At depths of 10 and 20 km (Figure 4), continental Antarctica is entirely crustal; however, over most of the oceanic regions these depths coincide with the base of the crust or the upper mantle. *An et al.* [2015] reported

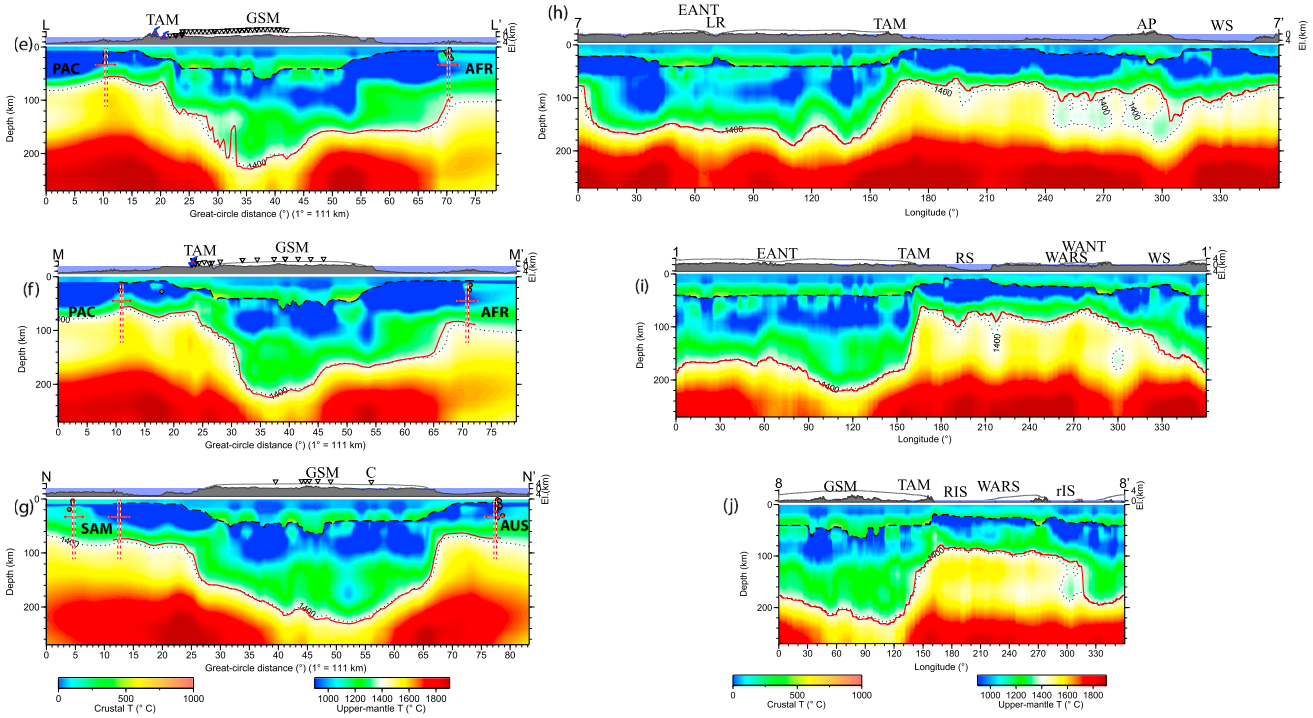

Figure 5. (continued)

large lateral variations in velocity beneath the Antarctic region (e.g., low beneath East Antarctica, high beneath oceanic regions); however, temperature variations between continental and oceanic regions are relatively small. High temperatures occur beneath ridges and at some hotspots at 10 and 20 km depth (e.g., the Balleny and St. Paul-Amsterdam hotspots), as well as beneath most volcanoes at 20 km depth. The West Antarctic rift system is hotter than surrounding regions at 20 km depth.

3.1.3. Representative Vertical Transects

Relatively low temperatures at depths of ≥150 km beneath some ridges (e.g., Figures 5a and 5b) may be an artifact. The ridges are boundaries of the Antarctic Plate with neighboring plates, but most the neighboring plates are not covered by our surface wave observations [*An et al.*, 2015, Figure 3]. Therefore, the upper mantle *S* velocities in AN1-S beneath those plates are mostly close to those in the 1-D global reference model, IASPEI91 [*Kennett and Engdahl*, 1991], which is used in the inversion for AN1-S. However, the real upper mantle *S* velocities beneath a ridge can be lower than those in IASPEI91. Furthermore, few surface wave dispersion measurements at periods of ≥150 s across ridges (suppporting information Figure S2b) were used in the inversion for the AN1-S model, indicating that the velocities at depths of approximately ≥150 km beneath ridges result mainly from lateral smearing from neighboring regions and plates.

At depths of 100–200 km, adiabatic temperatures of 1370−1420°C are associated with a mantle potential temperature of ~1330°C; consequently, the 1400°C isotherm (marked in Figure 5) is located near the thermal LAB, especially beneath East Antarctica where the lithosphere can be >100 km thick (Figure 2a). The depth of the 1400°C contour varies in different tectonic units. For example, from the South Pole to the St. Paul-Amsterdam hotspot (A-A′, Figure 5a), the contour gradually shallows from its deepest point (~150–200 km) beneath the Gamburtsev Subglacial Mountains to its shallowest point (~65 km) beneath the St. Paul-Amsterdam hotspot.

Since the thickness of oceanic lithosphere increases with age (supporting information Figure S1a), we expect the isothermal contour to deepen beneath oceanic regions. This occurs between the St. Paul-Amsterdam hotspot and the Kerguelen Plateau along transect A-A′ (Figure 5a), within 800 km of the ridge close to "B" or within 500 km of the ridge close to "B" along transect B-B′ (Figure 5b), close to "C" and the mid-Atlantic ridge along transect C-C′ (Figure 5c), and close to "L" and the Pacific-Antarctic ridge along transect L-L′ (Figure 5e). However, the 1400°C contour does not deepen with increasing crustal age close

to the Chile ridge ("A" in Figure 5a), in the Antarctic plate close to the American-Antarctic ridge (transect C-C', Figure 5c), close to the Australian-Antarctic ridge (D-D', Figure 5d), and between the African-Antarctic ridge (also called the Southwest Indian ridge; close to "L" and East Antarctica (L-L', Figure 5e). In these regions, isotherms for temperatures of $<$1400°C may vary laterally with crustal age, e.g., in the Antarctic Plate close to the American-Antarctic ridge (Figure 5c) and close to "A" in Figure 5a.

The 1400°C contour beneath West Antarctica (A-A', Figure 5a), especially beneath volcanoes, is shallow (~80 km) and similar to the contours beneath oceanic regions. A prominent high-temperature anomaly occurs as shallow as ~90 km beneath the West Antarctic rift system, and the margin of the anomaly is very sharp just beneath the Transantarctic Mountains (B-B', Figure 5b). The high-temperature anomaly beneath West Antarctica is isolated from the oceanic region by a cold segment along the continental margin and old oceanic lithosphere (Figure 5a). Temperature anomalies beneath the Transantarctic Mountains are similar to those beneath volcanoes and the West Antarctic rift system (Figures 5b and 5e) and likely represent a remnant of past thermal activity in this region.

A high-temperature layer at ~100 km depth separates two cold upper mantle layers beneath the Antarctic Peninsula (D-D', Figure 5d). The deeper cold layer is also observed at 150 km depth on the temperature map (Figure 3b). This layer is unlikely to be lithospheric, as ~150 km is generally too thick for young lithosphere. More likely, the upper boundary (at ~80 km depth) of the hot layer is the base of the lithosphere, which is similar to analogous young lithosphere in the North China basin [*An and Shi*, 2006; *An et al.*, 2009] and West Antarctica (Figure 2b).

The 1400°C isotherms beneath most of the volcanoes (e.g., Figures 5a, 5c, and 5e) and the St. Paul-Amsterdam hotspot have narrow bell-shaped trends with the peak just beneath the volcano, indicating that the magmas are derived from the asthenosphere and that the lithosphere thickens sharply away from the volcanoes. The 1400°C isotherm is shallow (~60 km) beneath the volcanoes and hotspots (e.g., the intraoceanic Balleny hotspot, Figure 5c; the St. Paul-Amsterdam hotspot in A-A', Figure 5a), even shallower than beneath oceanic ridges, which implies that the asthenosphere beneath hotspots or volcanoes is more destructive (i.e., hotter) than beneath a ridge and therefore has a greater influence on the overlying lithosphere.

The lateral variations in isotherms beneath hotspots and mid-ocean ridges seem counterintuitive, as the lithosphere beneath oceanic ridges is unexpectedly thick. This result may reflect the lower resolution of our model in oceanic regions; however, the resolving power of the dispersion measurements at periods of $\leq$100 s (supporting information Figure S2a) is better than at longer periods in oceanic regions, and the structure of oceanic lithosphere is effectively resolved because its thickness is generally $<$100 km. For example, close to the St. Paul-Amsterdam hotspot (Figure 5a), our model shows a thin lithosphere and sharp variations in thickness with crustal age, indicating that the model resolves upper mantle features in an oceanic region and can define lithosphere thickness-age relationships.

3.2. LAB Topography

The LAB depth (Figure 5) beneath the Antarctic Plate is calculated from AN1-Ts. Along transect A-A' (Figure 5a) the thickness of the lithosphere decreases gradually from East Antarctica ($>$200 km), across the Kerguelen Large Igneous Province, the oceanic floor, and the mid-oceanic ridge to the St. Paul-Amsterdam hotspot (~40 km). The resultant LAB model beneath Antarctica is called AN1-LAB (Figure 6).

At LAB depths, a temperature increase (or decrease) of 150°C, which is the uncertainty in calculated temperatures, results in a decrease (or increase) of ~15$-$30 km for the estimated depth of the LAB (Figure 2), defining the vertical uncertainty in AN1-LAB. Considering that Rayleigh waves at periods of 100 and 150 s have high sensitivity at ~100 and ~150 km depth, respectively, the resolution maps of 100 and 150 s (supporting information Figures S2a and S2b) are considered the lower bound in the lateral resolution of AN1-LAB.

Most of the lithosphere of East Antarctica, which is the oldest in Antarctica, is very thick (~150–250 km, Figure 6), with the greatest thickness (~250 km) between Domes A and C (Figures 5g and 6). The LAB in West Antarctica and oceanic regions (Figure 6) is ~60–110 km deep; however, beneath old (~100 Ma) oceanic regions in the eastern Antarctic Plate, the LAB is ~140 km deep. West Antarctica has a young ($<$ ~110 Ma) continental lithosphere that is thinner than the old ($>$100 Ma) oceanic lithosphere that surrounds East Antarctica. The lithosphere beneath volcanoes and hotspots (supporting information Figure S3) is very thin (~60 km). The LAB appears to be deep beneath the Antarctic Peninsula (Figure 6), where the lithosphere

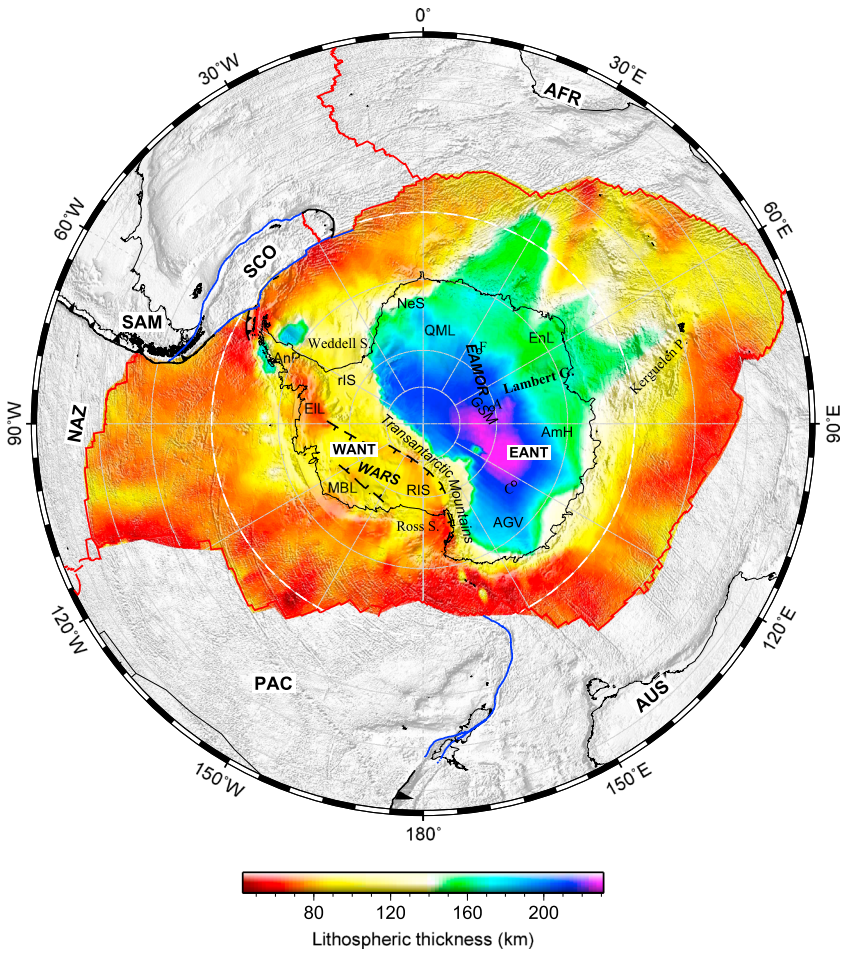

Figure 6. Topographic map of the Antarctic Plate LAB. The LAB base is defined as the shallowest position with a temperature crossing the 1330°C adiabat. Other symbols are as in Figure 1.

may be not so thick. A high-temperature layer at ~100 km depth (D-D'; Figure 5d) separates two cold upper mantle layers beneath the peninsula. The deep LAB in Figure 6 is based on the lower cold layer, which may represent subducted lithosphere (see section 4.3).

3.3. Curie Temperature Isotherm Map

The Curie temperature depth provides valuable information for assessing the geothermal potential, geodynamic evolution, and thermal conductivities of a region [*Rajaram*, 2007], as well as for interpreting magnetic anomalies. Aeromagnetic measurements can constrain Curie isotherm depths, but there is limited coverage in Antarctica [*Maule et al.*, 2005]. Using the steady state temperatures in AN1-Tc, we generated a Curie temperature depth map (Figure 7) with full coverage of the Antarctic Plate, assuming a Curie temperature of 580°C. All temperatures in AN1-Tc to a depth of 50 km are calculated from crustal information and from upper mantle temperatures (AN1-Ts) at 50–95 km depth. The upper mantle temperatures are derived from the *S* velocities (AN1-S) at 50–95 km depth, which are inverted from Rayleigh waves. Considering that Rayleigh waves at a period of 100 s include average *S* velocity information down to ~100 km, the resolution maps at 100 s (supporting information Figure S2a) are considered the lower bound of resolution for the Curie isotherm.

Beneath Antarctica, Curie temperature isotherms are mostly at depths of 10–40 km (Figure 7). For oceanic regions, Curie isotherms are consistent with crustal ages (supporting information Figure S1a). For example, the Curie temperature depth in both the western and eastern Antarctic areas with an oceanic crustal age of >50 Ma is mostly >25 km, and the depth in younger areas is <25 km. The Curie isotherm beneath the old cratonic East Antarctica region is >25 km deep, compared with <25 km beneath West Antarctica.

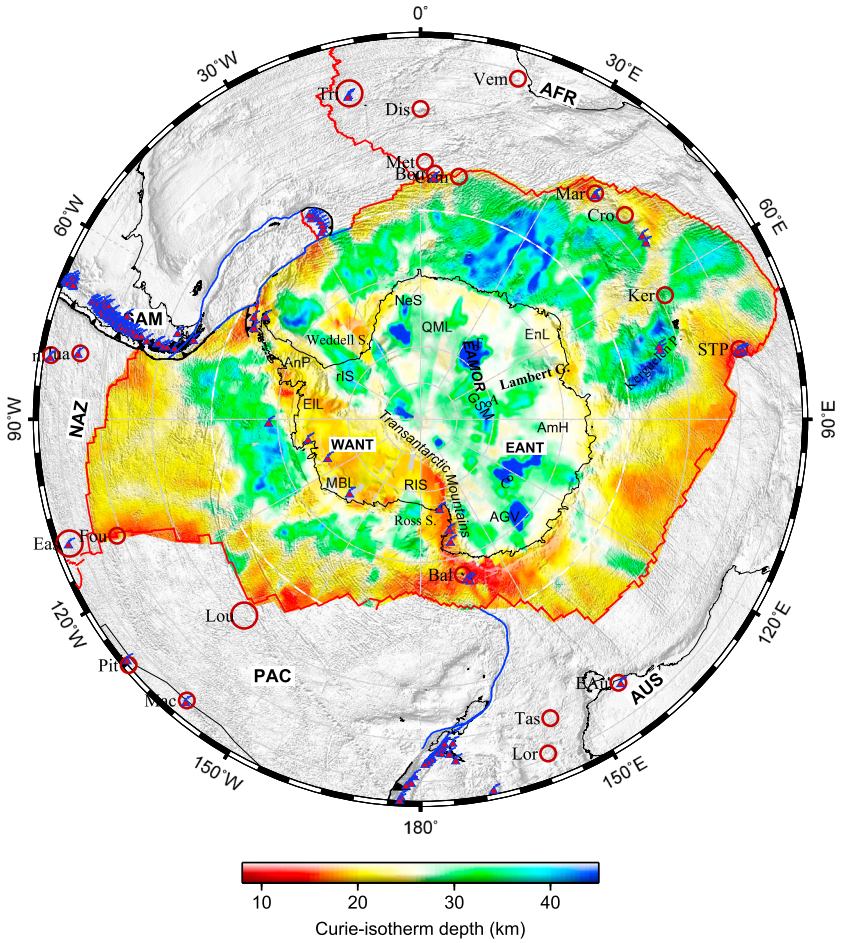

Figure 7. Map of the Curie temperature (580°C isotherm) depth of the Antarctic Plate. Symbols are as in Figure 1.

The Curie temperature depth is shallowest beneath hot spots such as the St. Paul-Amsterdam and Balleny hotspots.

3.4. Surface Heat Flux

Heat fluxes in oceanic regions have been well studied for geothermal assessments, although the resolution of our model is low in oceanic regions. Therefore, we only introduce heat flux results for continental Antarctica (Figure 8). Similar to Curie isotherms, the resolution maps at 100 s (supporting information Figure S2a) are considered the lower resolution bounds of heat flux results. *Maule et al.* [2005] proposed a heat flux model (supporting information Figure S4b) covering continental Antarctica by assuming a temperature of 0°C at the bedrock surface and a temperature of 580°C at either the magnetic crustal base (from sparse aeromagnetic measurements) or the seismic crustal base from an old global-scale seismic model of 3SMAC [*Nataf and Richard*, 1996]. There are clear differences between the two models (supporting information Figure S4); e.g., a prominent anomaly from the Ross Ice Shelf (RIS) to the Ronne Ice Shelf (rIS) [*Maule et al.*, 2005] was not observed in our model.

In our results, the heat flux in East Antarctica is $<65\ \mathrm{mWm^{-2}}$, which is the continental average [*Pollack et al.*, 1993], and the lowest heat fluxes are located close to Domes A, F, and C (Figure 8), where high ice sheet topography may depend on the low-geothermal heat flux. The heat flux in West Antarctica generally is higher than the continental average ($65\ \mathrm{mWm^{-2}}$). High heat flux also occurs along the boundary between the West Antarctic rift system and the Transantarctic Mountains.

An extraordinarily high-geothermal heat flux of ~$240\ \mathrm{mWm^{-2}}$ was directly measured in an ice core on the West Antarctic Ice Sheet Divide [*Clow et al.*, 2012]. This flux cannot be resolved by our model because our

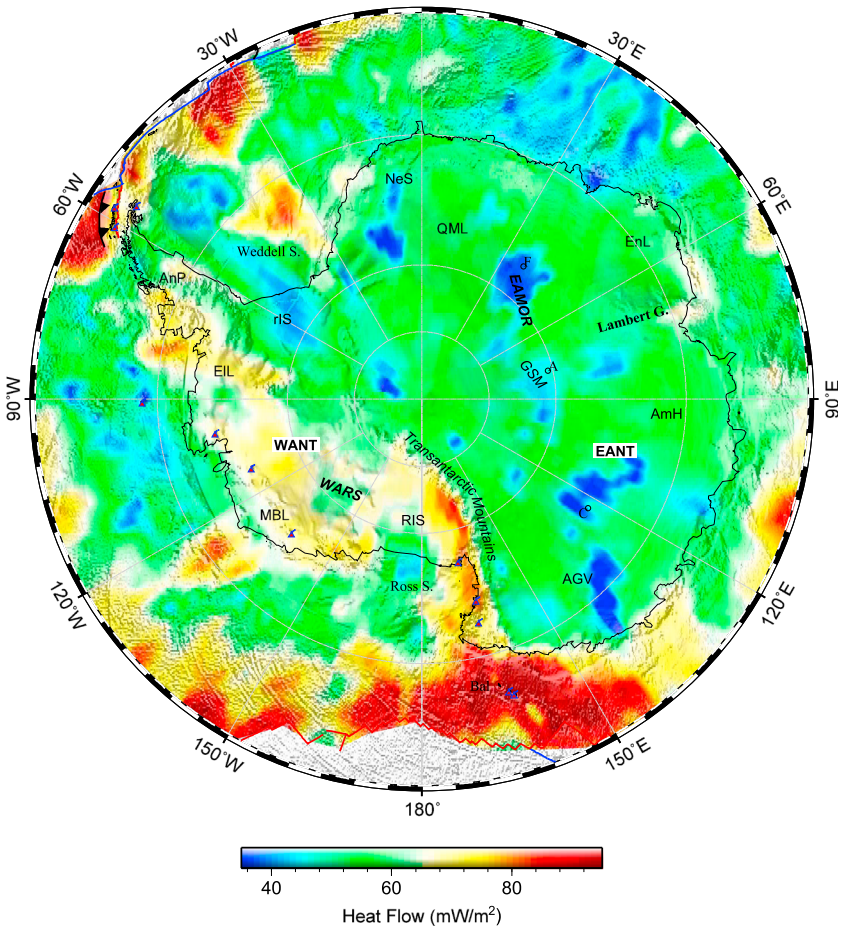

Figure 8. Map of heat flow in Antarctica. Symbols are as in Figure 1.

steady state thermal calculation is only valid if the heat flux is $< \sim 90\,\mathrm{mWm}^{-2}$, and the spatial extent of the high-flux anomaly may be smaller than the resolution of our model.

4. Discussion

4.1. Existence of Fluids in the Asthenosphere

The lithosphere is considered decoupled from the weaker asthenosphere, but the mechanism that underlies the decrease in material strength at the lithosphere-asthenosphere boundary remains debated [*Green et al.*, 2010; *Karato*, 2012]. The top of the asthenosphere has been defined by the onset of partial melting [*Anderson and Sammis*, 1970; *Anderson and Spetzler*, 1970; *Lambert and Wyllie*, 1970], but the existence of melting is a topic of controversy [e.g., *Priestley and McKenzie*, 2006]. Magnetotelluric studies indicate a high-electrical conductivity in the seismic LVZ, which may indicate hydrous/partial melt in the asthenosphere [e.g., *Presnall et al.*, 1972; *Drury*, 1978; *Evans et al.*, 2005; *Ni et al.*, 2011; *Naif et al.*, 2013]. In terms of seismology, a sharp negative velocity contrast at the LAB below the Pacific Plate, measured by high-frequency SS precursors, indicates the presence of melt at the top of the asthenosphere [*Schmerr*, 2012]. Low *S* velocities in the LVZ may also signal the presence of melt, but the amount of melt that does not completely wet grain boundaries ($<$0.1%) [e.g., *Hirschmann*, 2010] is so small that it would lead to very small reductions in seismic wave velocities [*Karato*, 2012]. The joint analysis of attenuation and seismic velocities may help to identify melt in the asthenosphere [*Yang and Forsyth*, 2008].

In our model, temperatures in the LVZ are equal to or higher than the dry solidus (Figures 2 and 3), thereby providing strong evidence for partial melting. Given that the relationships used to derive the temperatures do not consider the effect of melt, the high temperatures may overestimate the actual mantle temperature,

which also implies the existence of melts. Overall, the high temperatures below the LAB in our model are consistent with the existence of partial melt and support the idea that thermal weakening plays an important role in the movement of tectonic plates over the asthenosphere.

4.2. Relationship Between Thermal Structure and Tectonics

The lithosphere generally cools with time because of the release of heat by conduction, resulting in thickening of the lithosphere. Conductive cooling and thickening of continental lithosphere is a slow process. For example, if 250 km thick Precambrian lithosphere formed by the cooling of 100 km thick lithosphere at >550 Ma, then the thickening rate for that lithosphere is <30 km/100 Myr. This estimate is an upper bound because lithosphere older than 550 Ma is seldom thicker than 250 km. The slow cooling enables high-temperature anomalies beneath a rift region to be detected for >10 Myr after tectonic activity has ceased.

The thick crustal belt of the East Antarctic Mountain ranges (EAMOR) likely formed when East Gondwana was overthrust onto a continent composed of Indo-Antarctica and West Gondwana at ~500–550 Ma [*An et al.*, 2015]. In this case, the lithosphere beneath East Antarctica should be much older than the mountain ranges (i.e., the lithosphere should be >550 Ma). *Heeszel et al.* [2013] compared the phase velocity curves for East Antarctica with those in other tectonic belts and found the closest correspondence to early Proterozoic and Archean cratons. The thickest lithosphere (~250 km) of Antarctica is not located in but adjacent to regions with the thickest crust (e.g., the Gamburtsev Subglacial Mountains), which would mean that the thick lithosphere close to EAMOR appears to be the result of lithospheric doubling [*An et al.*, 2015], as reported for the Tibetan Plateau [*An and Shi*, 2006; *Feng et al.*, 2010]. In summary, the lithosphere of East Antarctica became thickened over a long period of cooling, and near EAMOR it thickened by lithospheric doubling during continent-continent collision.

The West Antarctic rift system underwent extension through much of the Cenozoic [e.g., *Granot et al.*, 2010], and the resulting thermal anomaly still persists in the asthenosphere. Most of West Antarctica also has a thin lithosphere (~90 km), similar to that of present-day rifts (e.g., the North China basin [*An and Shi*, 2006; *An et al.*, 2009]). Although no active volcanism is observed near the Transantarctic Mountains (inset in Figure 5), the mantle thermal anomalies beneath the Transantarctic Mountains (B-B′ and 8-8′ in Figure 5) are similar to those beneath active Antarctic volcanoes and beneath the West Antarctic rift system (A-A′ and L-L′ in Figure 5).

The term "hot spot" is commonly applied to any long-lived volcanic center that is not part of the global network of mid-ocean ridges and island arcs; however, the term is used rather loosely, and there is little agreement on the total number of hot spots worldwide [*Schubert et al.*, 2001]. For example, the Amsterdam and St. Paul Islands hotspot [*Anderson and Schramm*, 2005] is not associated with a large igneous province, and therefore, it has been excluded from some recent lists of hotspots [*Courtillot et al.*, 2003; *McNutt and Caress*, 2009]. Our temperature model provides insight into the Antarctic Plate hotspots (e.g., the Balleny, Marion, and St. Paul-Amsterdam hotspots). High-temperature anomalies beneath these hotspots extend from shallow depths (<100 km) to the lowest well-resolved depths (~250 km) and likely originate from at least 300 km depth.

Heat flux may play a major role in the formation of subglacial lakes [*Siegert and Dowdeswell*, 1996; *Siegert*, 2000; *Pollard et al.*, 2005]; however, we did not find a direct relationship (supporting information Figure S4) between heat flux and the number of subglacial lakes [*Siegert*, 2000; *Siegert et al.*, 2005; *Wright and Siegert*, 2012], probably due to the strong effect of ice thickness and topography on lake formation. On the other hand, the heat flux at topographic highs of the ice surface (e.g., Domes A, C, and F) is very low, and a correlation between geothermal heat flux and ice sheet topography may exist on a large scale.

4.3. Remnants of an Ancient Subduction System in West Antarctica

4.3.1. Arc and Back Arc of a Mesozoic Subduction System

Beneath the West Antarctic rift system, the temperatures at 100–150 km depth (Figure 2b) are equal to or higher than the dry mantle solidus, indicating the occurrence of partial melting, whereas at 150–200 km depth the temperatures are 100°C lower than the overlying material.

No previous study has imaged a slab in the mantle beneath West Antarctica [*Hansen et al.*, 2014], but an oceanic subduction zone existed in this region prior to ~50 Ma, along the continental borders close to Marie Byrd Land, Ellsworth Land, and the Antarctic Peninsula [*McCarron and Larter*, 1998; *Larter et al.*, 2002; *Siddoway*, 2008; *Torsvik et al.*, 2008] (supporting information Figure S5). The submarine bedrock of West

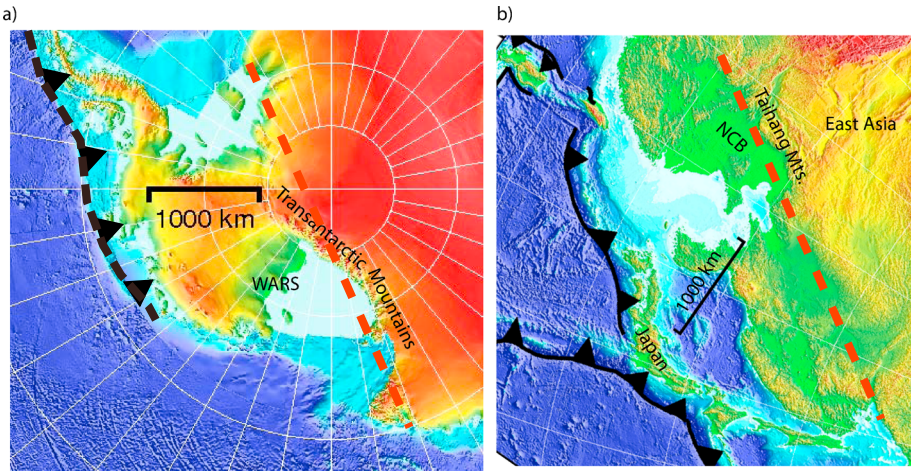

Figure 9. Comparison of the subduction systems of (a) Mesozoic West Antarctica and (b) present-day East Asia. NCB = North China rift basin; TAM = Transantarctic Mountains; and WARS = West Antarctic rift system.

Antarctica could have been a back-arc basin associated with this subduction zone along the paleo-Pacific coast of Gondwana [*Sutherland*, 2008; *Faure and Mensing*, 2010 and references therein]. Since New Zealand rifted from Marie Byrd Land at ~83 Ma, tectonism in Antarctica has generally been limited to extension and volcanism in the West Antarctic rift system. Given the slow conductive cooling/heating (as introduced above) and weak tectonic activity [*Winberry and Anandakrishnan*, 2003; *Reading*, 2007; *LeMasurier*, 2008] in West Antarctica during the Cenozoic, the end-Mesozoic topography of West Antarctica is likely to have been similar to that of today, except for the presence of a subduction zone trench (Figure 9a).

In an oceanic subduction system, the downgoing lithosphere becomes dehydrated, and the water expelled is concentrated at depths of 100–150 km, i.e., the top of the asthenosphere [*Finn et al.*, 2005]. The anomalously high temperatures beneath the West Antarctic rift system at 100–150 km depth (Figure 2b) may be the result of past subduction, and the relatively low temperature layer at 150–200 km depth or the cold bodies at 100–200 km depth west of the West Antarctic rift system (Figures 5a and 5b) may be the >50 Ma remnant of the cold, subducted slab.

Topographic and tectonic features (subduction-basin-mountain) in the West Antarctic rift-Transantarctic Mountains system (Figure 9a) are similar to those of the present-day Pacific subduction-North China basin-Taihang Mountains system (Figure 9b). Like the Mesozoic West Antarctic basin, the North China basin is a rift, and the thickness of crust [*An et al.*, 2015] and lithosphere (this study) beneath the West Antarctic rift system is similar to that of the North China basin [*Jia and Zhang*, 2005; *An and Shi*, 2006; *An et al.*, 2009]. Furthermore, the distance from the Transantarctic Mountains to the Mesozoic subduction zone was ~2000 km [*Siddoway*, 2008], which is similar to the distance between the Taihang Mountains and the Pacific subduction zone. These similarities suggest that the geodynamical processes in East Asia may be a modern analog for Mesozoic West Antarctica. For example, a vertical throw of >5 km across the Cenozoic piedmont fault zone separates the Taihang Mountains and the North China basin [*Xu et al.*, 2001]. Similarly, the ~4 km topographic difference between bedrock of the Transantarctic Mountains and the West Antarctic rift system may have resulted from continuous subsidence during and following subduction.

A large horizontal temperature difference in the upper mantle beneath thick and thin lithosphere favors edge-driven convection [*King and Anderson*, 1995, 1998; *King*, 2011]. Beneath Antarctica, a large horizontal temperature discrepancy at 100–200 km depth (Figures 5a and 5b) underneath the thick East Antarctic lithosphere and the thin West Antarctic lithosphere indicates that edge-driven convection can occur beneath the West Antarctic rift system (supporting information Figure S6). The convection can also result in a thermal anomaly beneath the West Antarctic rift system and a sharp shift in upper mantle temperatures beneath the Transantarctic Mountains following the cessation of subduction. In summary, a dynamic edge-driven convection process may have reinforced the thermal anomaly (Figures 5a and 5b) beneath the West Antarctic rift system and Transantarctic Mountains as observed in temperature images.

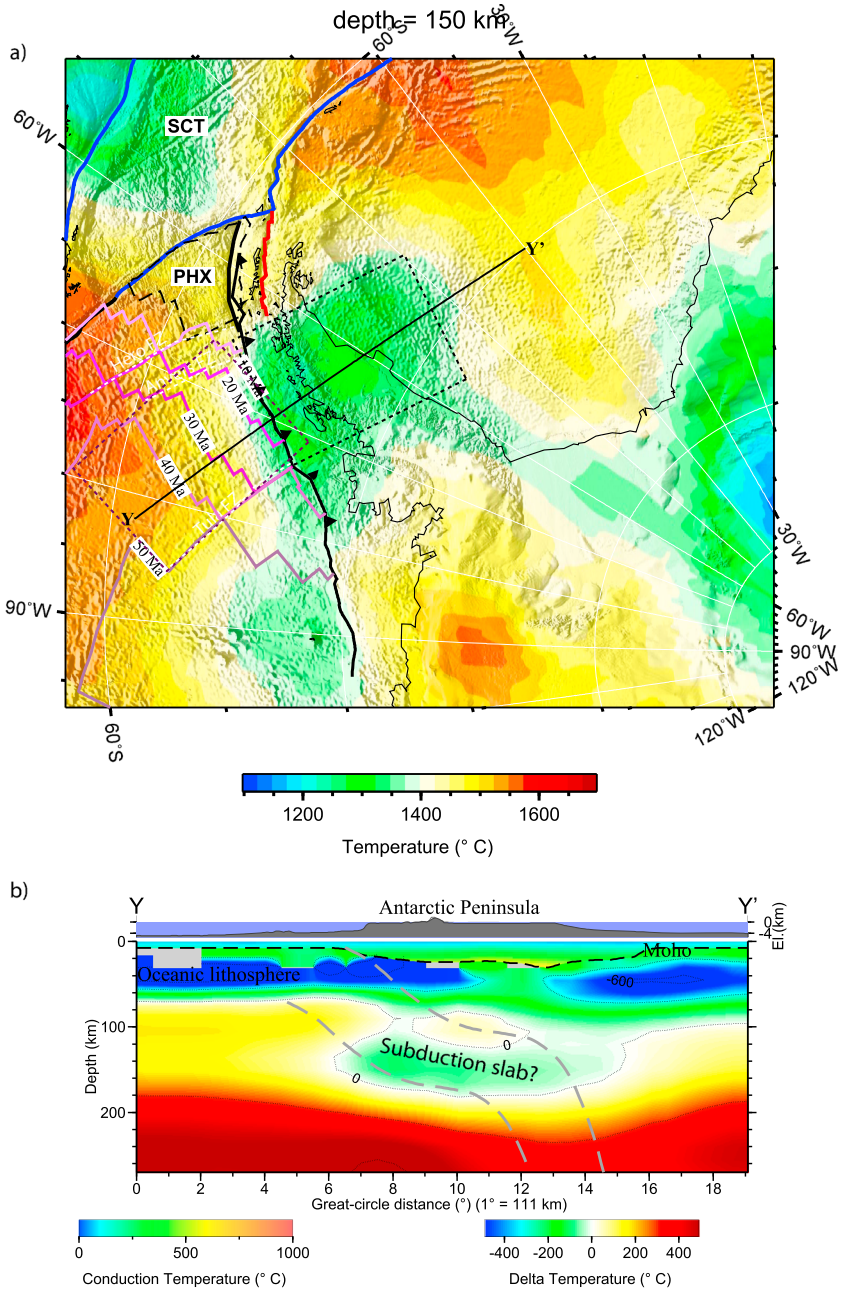

Figure 10. Temperatures beneath the Antarctic Peninsula: (a) at a depth of 150 km, and (b) in cross section. Two dashed squares in Figure 10a mark crustal displacement with convergence between oceanic lithosphere and the Antarctic Peninsula. Age-labeled color lines indicate the location [from *Eagles et al.*, 2009] of the reconstructed oceanic ridge at each time point. Other symbols in Figure 10a are as in Figure 1. The location of the section Y-Y' in Figure 10b is marked in Figure 10a. In Figure 10b, upper mantle temperature is the temperature anomaly ("delta temperature") relative to the adiabat of mantle potential temperature. The two gray dashed lines, which follow the geometry of the Peruvian flat slab at ~5°S [*Hayes et al.*, 2012], represent the upper and lower boundaries of a stalled slab beneath the Antarctic Peninsula.

4.3.2. Fossil Slab Beneath the Antarctic Peninsula

The Phoenix Plate was subducted under the Antarctic Peninsula for 100 Myr, and the last stage of that subduction system prior to 3 Ma (Figure 10a) was restricted to the northern tip of the peninsula [*Larter and Barker*, 1991; *Birkenmajer*, 1994; *Livermore et al.*, 2000; *Eagles et al.*, 2009; *Vérard et al.*, 2012]. Previous studies have shown that surface wave measurements are able to detect a stalled slab several million years after the end of subduction [e.g., *Wang et al.*, 2013].

A low-temperature region exists beneath the Antarctic Peninsula at a depth of 150 km (Figures 3 and 10a). In Transect D-D′ (Figure 5d), a high-temperature layer at ~100 km depth beneath the Antarctic Peninsula separates two cold upper mantle layers. If the lower cold layer is considered part of the lithosphere, the resultant lithosphere thickness (~150 km) is too thick for young continental lithosphere. On the other hand, if the high temperatures at 100 km depth mark the asthenosphere, then the Antarctic Peninsula lithosphere is ~80 km thick, and the deep cold upper mantle layer at 150 km depth could be the fossil subducted slab of the Phoenix Plate (Figure 10a).

The Phoenix Plate moved slowly relative to the Antarctic Plate, at ~24–75 km/Myr over the past 20 Myr [*Breitsprecher and Thorkelson*, 2009] and finally became extinct at ~3.3 Ma [*Fretzdorff et al.*, 2004]. The correlation between slab dip and the absolute motion of the overriding plate, as given in *Lallemand et al.* [2005], indicates that subduction of the Phoenix Plate was nearly flat beneath the Antarctic Peninsula. The cold region beneath the Antarctic Peninsula (Y-Y′, Figure 10b) is at similar depths and has a similar lateral extent as the flat slab beneath the Andes, supporting the idea that it is a remnant of the Phoenix slab. The cold anomaly related to the stalled slab persists beneath the Antarctic Peninsula to at least 200 km depth (Figure 10b). The slab segment close to "Y′" in Figure 10 could mark the position of the subduction trench at ~50 Ma, indicating that subduction of the slab segment within the area marked by the dashed square in the figure began no later than ~50 Ma and may have ceased by ~10 Ma. The horizontal extent of the slab is ~800 km (Figure 10), indicating an average convergence rate of ~20 km/Myr between 10 and ~50 Ma.

The cold body, or fossil slab, beneath the Antarctic Peninsula (Figure 10b) is disconnected from the shallow oceanic lithosphere beneath the western Antarctic Peninsula. Detachment of a sinking oceanic slab from the overriding plate indicates that subduction ceased because the "pull" from the older edge of the oceanic slab was no longer a driving force [*Burkett and Billen*, 2009]. The gap between the stalled slab and overriding plate may be a slab window associated with final subduction of the Phoenix spreading ridge, like those beneath southern South America [*Forsythe et al.*, 1986; *Breitsprecher and Thorkelson*, 2009]. If the cold body is the stalled slab, then the hot material (Figure 10b) just above the cold body should contain large amounts of fluid (mainly water) released from the subducted oceanic slab upon dehydration.

4.4. Is the Rate of Cooling of Oceanic Lithosphere Dependent on the Ridge Spreading Rate?

The cooling of oceanic lithosphere as it spreads away from a mid-ocean ridge results in thickening and subsidence of the lithosphere [*Davis and Lister*, 1974; *Parsons and Sclater*, 1977; *Schroeder*, 1984], and a linear relationship ($H \sim t^{1/2}$) has been proposed between the thickness of the oceanic lithosphere (H, represented by the isotherm depth of a base-lithosphere temperature) and the age of ocean crust (t) [*Davis and Lister*, 1974; *Stein and Stein*, 1992; *Doin and Fleitout*, 1996; *McKenzie et al.*, 2005], where the crustal age is $<$70 Ma. However, for oceanic crust older than ~70−90 Ma, the relationship between crustal age, thickness, and heat flow breaks down [*Parsons and Sclater*, 1977; *Schroeder*, 1984; *Crosby et al.*, 2006]. Surface wave tomography [*Ritzwoller et al.*, 2004] has shown that isovelocity contours of the lithospheric upper mantle of the Pacific Plate flatten for crustal ages of $>$70–100 Ma, although such a flattening was not detected by *Maggi et al.* [2006].

Our model has lower resolution in oceanic regions compared with the continental parts of the Antarctica Plate. The model does, however, show lateral variations in upper mantle temperatures beneath young oceanic regions, e.g., close to the St. Paul-Amsterdam hotspot and the Australian-Antarctic ridge (or Southeast Indian ridge) (A-A′, Figure 5a). Therefore, our model allows us to define the relationship between lithosphere thickness and age in the Antarctic Plate. Except for crustal ages of ~50–70 Ma and $>$ ~130 Ma, the thickening of young Antarctic oceanic lithosphere (Figure 11a) shows a nearly linear relationship with age that differs from the relationships seen in LAB depth curves based on the GDH1 [*Stein and Stein*, 1992] and half-space cooling models.

The thermal structure of oceanic lithosphere is normally assumed to be only a function of age, independent of spreading rate. However, the processes of formation of oceanic crust are found to be dependent on the spreading rate, especially at ultraslow ($\leq$20 mm/yr) spreading ridges [*Dick et al.*, 2003; *Lizarralde et al.*, 2004; *Rubin and Sinton*, 2007; *Standish et al.*, 2008; *Li et al.*, 2015], suggesting that the lithosphere thickness-age relationship may also be dependent on spreading rate. Supporting information Figure S7 shows that oceanic lithosphere created at ridges with a spreading rate of $\leq$25 mm/yr is generally thick ($>$70 km), even for young ($<$30 Ma) lithosphere. The lithosphere created at ridges with a rate slower than 30 mm/yr does not thicken as the age increases up to 70 Ma, indicating a flat base for oceanic lithosphere created at ultraslow spreading

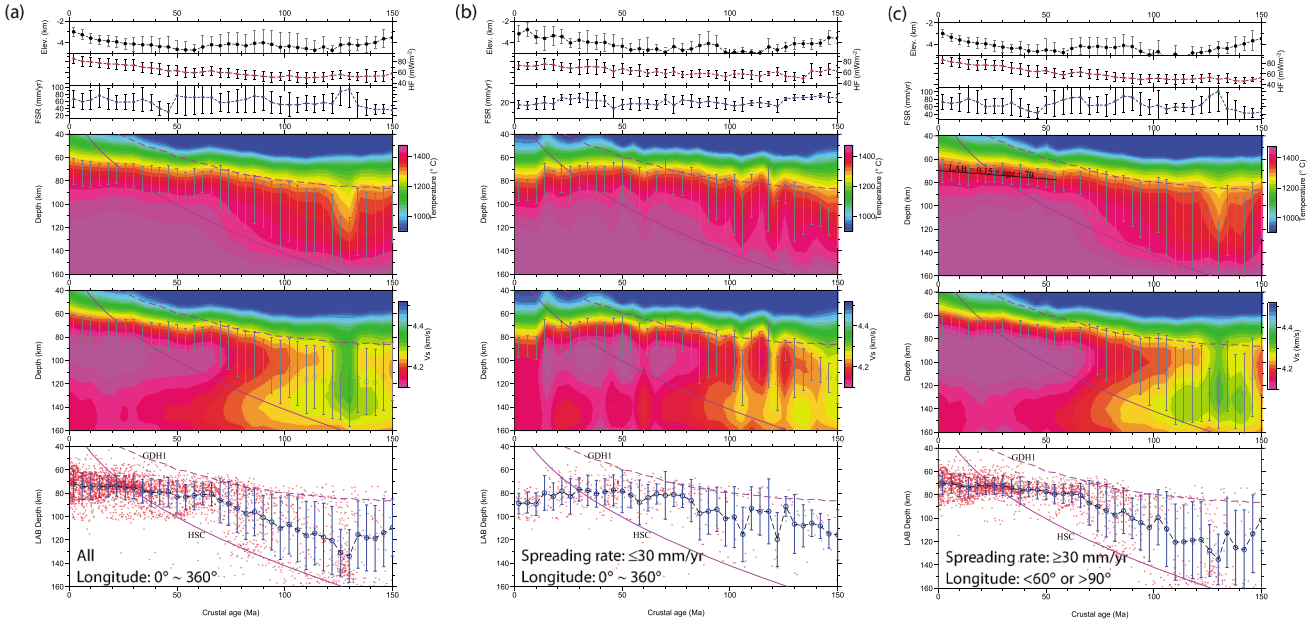

Figure 11. In each column, from top to bottom: average oceanic seafloor elevation, heat flux (HF), full spreading rate, deep temperature/*S* velocity, and LAB depth as a function of oceanic crustal age for (a) all oceanic crust, (b) crust created at slow ridges, and (c) all crust except that in Figure 11b and in the Kerguelen Plateau region ("D" in supporting information Figure S1a). Red circles represent the information of an equal-area cell in the oceanic region, and blue circles are mean values in 4 Myr bins, with error bars of one standard deviation about each mean value. Crustal age and spreading rate data are the same as in Figure S1, and lithospheric thicknesses are from Figure 6. Purple dashes represent the LAB determined from temperatures predicted by the GDH1 model, and the purple line is from temperatures predicted by the half-space cooling model, for which thermal diffusivity of the half space is 1×10^{-6} m^2 s^{-1}. The LAB definition for the curves is the same as for Figure 6, but different from *Stein and Stein* [1992]. The black line in Figure 11c and its regression equation represent the linear relationship between thickness and crustal age at ≤55 Ma.

ridges (Figures 11b and S8a in the supporting information). In terms of the average LAB-age relationship, the thickening rate (0.18 km/Myr, supporting information Figure S8a) is slower for lithosphere created at ridges with rates of 30–70 mm/yr compared with ridges with rates of >70 mm/yr (0.37 km/Myr, supporting information Figure S8c). In addition, the zero-age thickness of lithosphere that forms at fast-spreading ridges is thinner than that of lithosphere created at slower ridges (supporting information Figures S8a–S8c). Notably, the rate of lithosphere thickening increases during ~120–130 Ma, when the average spreading rate quickly increases; just after that time, the rate of lithosphere thickening distinctly decrease at ~130 Ma, when the average spreading rate suddenly decrease (Figure 11a). In summary, the cooling or thermal structure of oceanic lithosphere beneath the Antarctic Plate is dependent on the spreading rate of the ridge at which the lithosphere was produced. The oceanic lithosphere of the Antarctic Plate was created at several mid-oceanic ridges, indicating that the relationship between cooling and spreading rate shown here may be global in nature. Flattening (thickening rate decreased) of the Pacific lithosphere occurs when the spreading rate decreased between ~100 and ~70 Ma, indicating that cooling of the Pacific lithosphere was dependent on the spreading rate (supporting information Figure S9).

The sharp thickness variation at crustal ages of 50–70 Ma (Figure 11a) is similar to that found in the Pacific Plate where there is a sudden change in the rate of increasing lithosphere thickness [*Ritzwoller et al.*, 2004]; however, our results show a sharp fluctuation rather than an inflection in the flattened profile for the lithospheric base. A strong shift at ~50–70 Ma is also observed in the Kerguelen Large Igneous Province (supporting information Figure S10d and text), suggesting that the average plate variation reflects the local variation in the Kerguelen Large Igneous Province.

If we discard regions associated with the Kerguelen Plateau and those generated at ultraslow (<30 mm/yr) spreading centers, the average LAB-age relationship (Figure 11c) is linear for young lithosphere of the Antarctic Plate. The thickening rate of mature (> ~65 Ma) lithosphere is higher than that of young lithosphere (~0.15 km/Myr), even though mature oceanic lithosphere has typically experienced more tectonothermal events over a longer period of time. Our mean LAB curve for mature lithosphere lies between GDH1 and half-space cooling model curves, which are considered the upper and lower bounds of our model.

Of note, the LAB predicted by the GDH1 model (Figures 11a and 11c) is similar to the ~1000°C isotherm in our model, where the crust is <50 Ma. This indicates that our temperature model is consistent with the prediction of temperature variation by heat flow observations, but not with the LAB (e.g., GDH1 model). Furthermore, variability of the ~1000°C isotherm (Figure 11a) is generally similar to that of the surface elevation of crust of all ages, which indicates that seafloor topography, in addition to deep thermal structures, may also be related to the spreading rate of the ridge.

5. Conclusions

Using *S* velocities in the 3-D seismic model AN1-S, we calculated upper mantle temperatures of the Antarctic Plate on the basis of the thermoelastic properties of mantle minerals. Crustal temperatures and surface heat fluxes were calculated from upper mantle temperatures under the assumption of steady state thermal conduction. Our results give temperatures higher than the dry mantle solidus beneath the seismic LAB for some regions of the Antarctic Plate, indicating the presence of partial melt in the asthenosphere. Therefore, our results support the idea that thermal weakening of the asthenosphere plays an important role in the movement of tectonic plates.

Maps of the lithosphere-asthenosphere boundary depth and the Curie temperature isotherm were constructed from our calculated temperatures. The results indicate that the depth of the LAB for the Antarctic Plate is ~60–110 km beneath West Antarctica and oceanic regions, and ~150–250 km beneath East Antarctica, and that the thickest lithosphere (~250 km) is beneath Domes A and C in East Antarctica. The lithosphere beneath volcanoes and hotspots is very thin (~60 km).

Subduction occurred along the boundaries of West Antarctica until the early Cenozoic. If we superimpose a subduction zone on present-day West Antarctica, the topographic and tectonic features (subduction-basin-mountain) of the West Antarctic rift system-Transantarctic Mountains system are similar to those of the present-day Pacific subduction-North China basin-Taihang Mountains system. The similarities between the two tectonic systems indicate that geodynamical processes involved in the formation of West Antarctica may have been similar to those currently observed in East Asia. Our model points to the presence of a cold body beneath the Antarctic Peninsula, which is possibly a remnant subducted slab of the Phoenix Plate.

Oceanic lithosphere generally thickens as crustal age increases, and the rate of lithosphere thickening may be related to the spreading rate of the oceanic ridge where the lithosphere was generated. Large variability in age-thickness relationships occurs in the oceanic Kerguelen Large Igneous Province, possibly due to strong tectonothermal effects since the oceanic crust was formed. If we ignore the regions close to the Kerguelen Large Igneous Province and the St. Paul-Amsterdam hotspot, the age-thickness curve follows a nearly linear relationship for young lithosphere, but it follows a different linear relationship (without flattening) for mature oceanic lithosphere of the Antarctic Plate.

Acknowledgments

This work was funded by the National Natural Science Foundation of China (grant 40874021), Chinese Polar Environment Comprehensive Investigation and Assessment Programmes (CHINARE2013-04-02), Chinese IPY projects, and the U.S. National Science Foundation (grants ANT-0537597 and ANT-0632209). Detailed constructive comments from the Associate Editor and two anonymous reviewers helped improve the text. We thank the Associate Editor, Anya M. Reading, and an anonymous reviewer for numerous comments on our companion paper, *An et al.* [2015]. All figures were generated using Generic Mapping Tools [*Wessel and Smith*, 1991]. The temperature models and LAB-depth map are available through http://www.seismolab.org.

References

An, M. (2012), A simple method for determining the spatial resolution of a general inverse problem, *Geophys. J. Int.*, *191*, 849–864, doi:10.1111/j.1365-246X.2012.05661.x.

An, M., and Y. Shi (2006), Lithospheric thickness of the Chinese continent, *Phys. Earth Planet. Inter.*, *159*, 257–266, doi:10.1016/j.pepi.2006.08.002.

An, M., and Y. Shi (2007), 3D crustal and upper-mantle temperature of the Chinese continent, *Sci. China, Ser. D: Earth Sci.*, *50*, 1441–1451, doi:10.1007/s11430-007-0071-3.

An, M., M. Feng, and Y. Zhao (2009), Destruction of lithosphere within the north China craton inferred from surface wave tomography, *Geochem. Geophys. Geosyst.*, *10*, Q08016, doi:10.1029/2009GC002562.

An, M., D. A. Wiens, Y. Zhao, M. Feng, A. A. Nyblade, M. Kanao, Y. Li, A. Maggi, and J. Lévêque (2015), *S*-velocity model and inferred Moho topography beneath the Antarctic Plate from Rayleigh waves, *J. Geophys. Res. Solid Earth*, *120*, 359–383, doi:10.1002/2014JB011332.

Anderson, D. L., and C. Sammis (1970), Partial melting in the upper mantle, *Phys. Earth Planet. Inter.*, *3*, 41–50, doi:10.1016/0031-9201(70)90042-7.

Anderson, D. L., and H. Spetzler (1970), Partial melting and the low-velocity zone, *Phys. Earth Planet. Inter.*, *4*, 62–64, doi:10.1016/0031-9201(70)90030-0.

Anderson, D. L., and K. A. Schramm (2005), Global hotspot maps, *Geol. Soc. Am. Spec. Pap.*, *388*, 19–29, doi:10.1130/0-8137-2388-4.19.

Artemieva, I. M., and W. D. Mooney (2001), Thermal thickness and evolution of Precambrian lithosphere: A global study, *J. Geophys. Res.*, *106*, 16,387–16,414, doi:10.1029/2000JB900439.

Berckhemer, H., W. Kampfmann, E. Aulbach, and H. Schmeling (1982), Shear modulus and Q of forsterite and dunite near partial melting from forced-oscillation experiments, *Phys. Earth Planet. Inter.*, *29*, 30–41, doi:10.1016/0031-9201(82)90135-2.

Birkenmajer, K. (1994), Evolution of the Pacific margin of the northern Antarctic Peninsula: An overview (in English), *Geol. Rundsch.*, *83*, 309–321, doi:10.1007/bf00210547.
Breitsprecher, K., and D. J. Thorkelson (2009), Neogene kinematic history of Nazca–Antarctic–Phoenix slab windows beneath Patagonia and the Antarctic Peninsula, *Tectonophysics*, *464*, 10–20, doi:10.1016/j.tecto.2008.02.013.
Burkett, E. R., and M. I. Billen (2009), Dynamics and implications of slab detachment due to ridge–trench collision, *J. Geophys. Res.*, *114*, B12402, doi:10.1029/2009JB006402.
Cammarano, F., S. Goes, P. Vacher, and D. Giardini (2003), Inferring upper-mantle temperatures from seismic velocities, *Phys. Earth Planet. Inter.*, *138*, 197–222.
Cermak, V. (1982), Geothermal model of the lithosphere and the map of the lithosphere thickness for the USSR territory [in Russian], *Izv. Akad. Nauk SSSR Fiz. Zemli*, *11*, 25–38.
Clauser, C., and E. Huenges (1995), Thermal conductivity of rocks and minerals, in *Rock Physics and Phase Relations*, edited by T. J. Ahrens, pp. 105–126, AGU, Washington, D. C.
Clow, G. D., K. M. Cuffey, and E. D. Waddington (2012), High heat-flow beneath the central portion of the West Antarctic ice sheet, Abstract C31A-0577 paper presented at 2012 Fall Meeting, AGU, San Francisco, Calif., 3–7 Dec.
Courtillot, V., A. Davaille, J. Besse, and J. Stock (2003), Three distinct types of hotspots in the Earth's mantle, *Earth Planet. Sci. Lett.*, *205*, 295–308, doi:10.1016/s0012-821x(02)01048-8.
Crosby, A. G., D. McKenzie, and J. G. Sclater (2006), The relationship between depth, age, and gravity in the oceans, *Geophys. J. Int.*, *166*, 553–573, doi:10.1111/j.1365-246X.2006.03015.x.
Davis, E. E., and C. R. B. Lister (1974), Fundamentals of ridge crest topography, *Earth Planet. Sci. Lett.*, *21*, 405–413, doi:10.1016/0012-821X(74)90180-0.
de Jonge, M. R., M. J. R. Wortel, and W. Spakman (1994), Regional scale tectonic evolution and the seismic velocity structure of the lithosphere and upper mantle: The Mediterranean region, *J. Geophys. Res.*, *99*, 12,091–12,108, doi:10.1029/94JB00648.
Dick, H. J. B., R. L. Fisher, and W. B. Bryan (1984), Mineralogic variability of the uppermost mantle along mid-ocean ridges, *Earth Planet. Sci. Lett.*, *69*, 88–106, doi:10.1016/0012-821X(84)90076-1.
Dick, H. J. B., J. Lin, and H. Schouten (2003), An ultraslow-spreading class of ocean ridge, *Nature*, *426*, 405–412.
Doin, M. P., and L. Fleitout (1996), Thermal evolution of the oceanic lithosphere: An alternative view, *Earth Planet. Sci. Lett.*, *142*, 121–136, doi:10.1016/0012-821x(96)00082-9.
Drury, M. J. (1978), Partial melt in the asthenosphere: Evidence from electrical conductivity data, *Phys. Earth Planet. Inter.*, *17*, P16–P20, doi:10.1016/0031-9201(78)90045-6.
Eagles, G., K. Gohl, and R. D. Larter (2009), Animated tectonic reconstruction of the Southern Pacific and alkaline volcanism at its convergent margins since Eocene times, *Tectonophysics*, *464*, 21–29, doi:10.1016/j.tecto.2007.10.005.
Evans, R. L., G. Hirth, K. Baba, D. Forsyth, A. Chave, and R. Mackie (2005), Geophysical evidence from the MELT area for compositional controls on oceanic plates, *Nature*, *437*, 249–252, doi:10.1038/nature04014.
Fahnestock, M., W. Abdalati, I. Joughin, J. Brozena, and P. Gogineni (2001), High geothermal heat flow, basal melt, and the origin of rapid ice flow in central Greenland, *Science*, *294*, 2338–2342, doi:10.1126/science.1065370.
Faure, G., and T. M. Mensing (2010), *The Transantarctic Mountains: Rocks, Ice, Meteorites and Water*, 804 pp., Springer, Heidelberg.
Feng, M., S. van der Lee, M. An, and Y. Zhao (2010), Lithospheric thickness, thinning, subduction, and interaction with the asthenosphere beneath China from the joint inversion of seismic *S*-wave train fits and Rayleigh-wave dispersion curves, *Lithos*, *120*, 116–130, doi:10.1016/j.lithos.2009.11.017.
Finn, C. A., R. D. Müller, and K. S. Panter (2005), A Cenozoic diffuse alkaline magmatic province (DAMP) in the southwest Pacific without rift or plume origin, *Geochem. Geophys. Geosyst.*, *6*, Q02005, doi:10.1029/2004GC000723.
Forsythe, R. D., E. P. Nelson, M. J. Carr, M. E. Kaeding, M. Herve, C. Mpodozis, J. M. Soffia, and S. Harambour (1986), Pliocene near-trench magmatism in southern Chile: A possible manifestation of ridge collision, *Geology*, *14*, 23–27, doi:10.1130/0091-7613(1986)14<23:pnmisc>2.0.co;2.
Fretwell, P., et al. (2013), Bedmap2: Improved ice bed, surface and thickness datasets for Antarctica, *Cryosphere*, *7*, 375–393, doi:10.5194/tc-7-375-2013.
Fretzdorff, S., T. J. Worthington, K. M. Haase, R. Hékinian, L. Franz, R. A. Keller, and P. Stoffers (2004), Magmatism in the Bransfield Basin: Rifting of the South Shetland Arc?, *J. Geophys. Res.*, *109*, B12208, doi:10.1029/2004JB003046.
Frost, B. R., and P. N. Shive (1986), Magnetic mineralogy of the lower continental crust, *J. Geophys. Res.*, *91*, 6513–6521, doi:10.1029/JB091iB06p06513.
Fullea, J., J. C. Afonso, J. A. D. Connolly, M. Fernàndez, D. García-Castellanos, and H. Zeyen (2009), LitMod3D: An interactive 3-D software to model the thermal, compositional, density, seismological, and rheological structure of the lithosphere and sublithospheric upper mantle, *Geochem. Geophys. Geosyst.*, *10*, Q08019, doi:10.1029/2009GC002391.
Goes, S., and S. Van der Lee (2002), Thermal structure of the North American uppermost mantle inferred from seismic tomography, *J. Geophys. Res.*, *107*(B3), 2050, doi:10.1029/2000JB000049.
Goes, S., R. Govers, and P. Vacher (2000), Shallow mantle temperatures under Europe from *P* and *S* wave tomography, *J. Geophys. Res.*, *105*, 11,153–11,169, doi:10.1029/1999JB900300.
Granot, R., S. C. Cande, J. M. Stock, F. J. Davey, and R. W. Clayton (2010), Postspreading rifting in the Adare Basin, Antarctica: Regional tectonic consequences, *Geochem. Geophys. Geosyst.*, *11*, Q08005, doi:10.1029/2010GC003105.
Green, D. H., W. O. Hibberson, I. Kovacs, and A. Rosenthal (2010), Water and its influence on the lithosphere-asthenosphere boundary, *Nature*, *467*, 448–451, doi:10.1038/nature09369.
Hansen, S. E., J. H. Graw, L. M. Kenyon, A. A. Nyblade, D. A. Wiens, R. C. Aster, A. D. Huerta, S. Anandakrishnan, and T. Wilson (2014), Imaging the Antarctic mantle using adaptively parameterized *P*-wave tomography: Evidence for heterogeneous structure beneath West Antarctica, *Earth Planet. Sci. Lett.*, *408*, 66–78, doi:10.1016/j.epsl.2014.09.043.
Hasterok, D., and D. S. Chapman (2011), Heat production and geotherms for the continental lithosphere, *Earth Planet. Sci. Lett.*, *307*, 59–70, doi:10.1016/j.epsl.2011.04.034.
Hayes, G. P., D. J. Wald, and R. L. Johnson (2012), Slab1.0: A three-dimensional model of global subduction zone geometries, *J. Geophys. Res.*, *117*, B01302, doi:10.1029/2011JB008524.
Heeszel, D. S., D. A. Wiens, A. A. Nyblade, S. E. Hansen, M. Kanao, M. An, and Y. Zhao (2013), Rayleigh wave constraints on the structure and tectonic history of the Gamburtsev Subglacial Mountains, East Antarctica, *J. Geophys. Res. Solid Earth*, *118*, 2138–2153, doi:10.1002/jgrb.50171.
Hirschmann, M. M. (2010), Partial melt in the oceanic low velocity zone, *Phys. Earth Planet. Inter.*, *179*, 60–71, doi:10.1016/j.pepi.2009.12.003.

Hirth, G., and D. L. Kohlstedt (1996), Water in the oceanic upper mantle: Implications for rheology, melt extraction and the evolution of the lithosphere, *Earth Planet. Sci. Lett.*, *144*, 93–108.
Huang, Z., W. Su, Y. Peng, Y. Zheng, and H. Li (2003), Rayleigh wave tomography of China and adjacent regions, *J. Geophys. Res.*, *108*(B2), 2073, doi:10.1029/2001JB001696.
Ito, G., and P. E. van Keken (2007), Hot spots and melting anomalies, in *Treatise in Geophysics: Mantle Dynamics*, edited by D. Bercovici, pp. 371–435, Elsevier, Amsterdam.
Jaupart, C., and J. C. Mareschal (1999), The thermal structure and thickness of continental roots, *Lithos*, *48*, 93–114.
Jaupart, C., and J. C. Mareschal (2007), Heat flow and thermal structure of the lithosphere, in *Treatise on Geophysics*, edited by G. Schubert, pp. 217–251, Elsevier, Amsterdam.
Jia, S.-X., and X.-K. Zhang (2005), Crustal structure and comparison of different tectonic blocks in North China, *Chin. J. Geophys.*, *48*, 672–683.
Jordan, T. H. (1979), Mineralogies, densities and seismic velocities of garnet lherzolites and their geophysical implications, in *The Mantle Sample: Inclusions in Kimberlites and Other Volcanics*, edited by F. R. Boyd and H. O. A. Myer, pp. 1–14, AGU, Washington, D. C.
Kampfmann, W., and H. Berckhemer (1985), High temperature experiments on the elastic and anelastic behaviour of magmatic rocks, *Phys. Earth Planet. Inter.*, *40*, 223–247, doi:10.1016/0031-9201(85)90132-3.
Karato, S.-I. (1993), Importance of anelasticity in the interpretation of seismic tomography, *Geophys. Res. Lett.*, *20*, 1623–1626, doi:10.1029/93GL01767.
Karato, S.-I. (2012), On the origin of the asthenosphere, *Earth Planet. Sci. Lett.*, *321–322*, 95–103, doi:10.1016/j.epsl.2012.01.001.
Karato, S.-I., and H. Jung (1998), Water, partial melting and the origin of the seismic low velocity and high attenuation zone in the upper mantle, *Earth Planet. Sci. Lett.*, *157*, 193–207.
Katsura, T., A. Yoneda, D. Yamazaki, T. Yoshino, and E. Ito (2010), Adiabatic temperature profile in the mantle, *Phys. Earth Planet. Inter.*, *183*, 212–218, doi:10.1016/j.pepi.2010.07.001.
Katz, R. F., M. Spiegelman, and C. H. Langmuir (2003), A new parameterization of hydrous mantle melting, *Geochem. Geophys. Geosyst.*, *4*(9), 1073, doi:10.1029/2002GC000433.
Kennett, B. L. N., and E. R. Engdahl (1991), Traveltimes for global earthquake location and phase identification, *Geophys. J. Int.*, *105*, 429–465.
King, S. D. (2011), Volcanism: Eruptions above mantle shear, *Nat. Geosci.*, *4*, 279–280.
King, S. D., and D. L. Anderson (1995), An alternative mechanism of flood basalt formation, *Earth Planet. Sci. Lett.*, *136*, 269–279, doi:10.1016/0012-821X(95)00205-Q.
King, S. D., and D. L. Anderson (1998), Edge-driven convection, *Earth Planet. Sci. Lett.*, *160*, 289–296, doi:10.1016/S0012-821X(98)00089-2.
Lallemand, S., A. Heuret, and D. Boutelier (2005), On the relationships between slab dip, back-arc stress, upper plate absolute motion, and crustal nature in subduction zones, *Geochem. Geophys. Geosyst.*, *6*, Q09006, doi:10.1029/2005GC000917.
Lambert, I. B., and P. J. Wyllie (1970), Low-velocity zone of the Earth's mantle: Incipient melting caused by Water, *Science*, *169*, 764–766, doi:10.1126/science.169.3947.764.
Larter, R. D., and P. F. Barker (1991), Effects of ridge crest-trench interaction on Antarctic-Phoenix spreading: Forces on a young subducting plate, *J. Geophys. Res.*, *96*, 19,583–19,607, doi:10.1029/91JB02053.
Larter, R. D., A. P. Cunningham, P. F. Barker, K. Gohl, and F. O. Nitsche (2002), Tectonic evolution of the Pacific margin of Antarctica 1. Late Cretaceous tectonic reconstructions, *J. Geophys. Res.*, *107*(B12), 2345, doi:10.1029/2000JB000052.
LeMasurier, W. E. (2008), Neogene extension and basin deepening in the West Antarctic rift inferred from comparisons with the East African rift and other analogs, *Geology*, *36*, 247–250, doi:10.1130/g24363a.1.
Li, J., et al. (2015), Seismic observation of an extremely magmatic accretion at the ultraslow spreading Southwest Indian Ridge, *Geophys. Res. Lett.*, *42*, 2656–2663, doi:10.1002/2014GL062521.
Livermore, R., et al. (2000), Autopsy on a dead spreading center: The Phoenix Ridge, Drake Passage, Antarctica, *Geology*, *28*, 607–610, doi:10.1130/0091-7613(2000)28<607:aoadsc>2.0.co;2.
Lizarralde, D., J. B. Gaherty, J. A. Collins, G. Hirth, and S. D. Kim (2004), Spreading-rate dependence of melt extraction at mid-ocean ridges from mantle seismic refraction data, *Nature*, *432*, 744–747, doi:10.1038/nature03140.
Llubes, M., C. Lanseau, and F. Rémy (2006), Relations between basal condition, subglacial hydrological networks and geothermal flux in Antarctica, *Earth Planet. Sci. Lett.*, *241*, 655–662, doi:10.1016/j.epsl.2005.10.040.
Maggi, A., E. Debayle, K. Priestley, and G. Barruol (2006), Multimode surface waveform tomography of the Pacific Ocean: A closer look at the lithospheric cooling signature, *Geophys. J. Int.*, *166*, 1384–1397, doi:10.1111/j.1365-246X.2006.03037.x.
Maule, C. F., M. E. Purucker, N. Olsen, and K. Mosegaard (2005), Heat flux anomalies in Antarctica revealed by satellite magnetic data, *Science*, *309*, 464–467, doi:10.1126/science.1106888.
McCarron, J. J., and R. D. Larter (1998), Late cretaceous to early tertiary subduction history of the Antarctic Peninsula, *J. Geol. Soc. London*, *155*, 255–268, doi:10.1144/gsjgs.155.2.0255.
McDonough, W. F., and R. L. Rudnick (1998), Mineralogy and composition of the upper mantle, in *Ultrahigh-Pressure Mineralogy: Physics and Chemistry of the Earth's Deep Interior*, edited by R. J. Hemley, pp. 139–164, Mineralog. Soc. of Am., Washington, D. C.
McKenzie, D., J. Jackson, and K. Priestley (2005), Thermal structure of oceanic and continental lithosphere, *Earth Planet. Sci. Lett.*, *233*, 337–349, doi:10.1016/j.epsl.2005.02.005.
McNutt, M. K., and D. W. Caress (2009), Crust and lithosphere structure—Hot spots and hot-spot swells, in *Seismology and Structure of the Earth: Treatise on Geophysics*, edited by B. Romanowicz and A. Dziewonski, pp. 445–478, Elsevier, Amsterdam, Netherlands.
Minster, J. B., and D. L. Anderson (1981), A model of dislocation-controlled rheology for the mantle, *Phil. Trans. R. Soc. Lond. A*, *299*, 319–356.
Müller, R. D., J.-Y. Royer, and L. A. Lawver (1993), Revised plate motions relative to the hotspots from combined Atlantic and Indian Ocean hotspot tracks, *Geology*, *21*, 275–278, doi:10.1130/0091-7613(1993)021<0275:rpmrtt>2.3.co;2.
Naif, S., K. Key, S. Constable, and R. L. Evans (2013), Melt-rich channel observed at the lithosphere–asthenosphere boundary, *Nature*, *495*, 356–359, doi:10.1038/nature11939.
Nataf, H. C., and Y. Richard (1996), 3SMAC: An a priori tomographic model of the upper mantle based on geophysical modeling, *Phys. Earth Planet. Inter.*, *95*, 101–122.
Ni, H., H. Keppler, and H. Behrens (2011), Electrical conductivity of hydrous basaltic melts: Implications for partial melting in the upper mantle (in English), *Contrib. Mineral. Petrol.*, *162*, 637–650, doi:10.1007/s00410-011-0617-4.
Nolet, G., and A. Zielhuis (1994), Low *S* velocities under the Tornquist-Teisseyre zone: Evidence for water injection into the transition zone by subduction, *J. Geophys. Res.*, *99*, 15,813–15,820, doi:10.1029/94JB00083.
Parsons, B., and J. G. Sclater (1977), An analysis of the variation of ocean floor bathymetry and heat flow with age, *J. Geophys. Res.*, *82*, 803–827, doi:10.1029/JB082i005p00803.

Pinet, C., and C. Jaupart (1987), The vertical distribution of radiogenic heat production in the Precambrian crust of Norway and Sweden: Geothermal implications, *Geophys. Res. Lett.*, *14*, 260–263.
Pollack, H., S. Hurter, and J. Johnson (1993), Heat flow from the Earth's interior: Analysis of the global data set, *Rev. Geophys.*, *31*, 267–280.
Pollard, D., R. M. DeConto, and A. A. Nyblade (2005), Sensitivity of Cenozoic Antarctic ice sheet variations to geothermal heat flux, *Global Planet. Change*, *49*, 63–74, doi:10.1016/j.gloplacha.2005.05.003.
Presnall, D. C., C. L. Simmons, and H. Porath (1972), Changes in electrical conductivity of a synthetic basalt during melting, *J. Geophys. Res.*, *77*, 5665–5672, doi:10.1029/JB077i029p05665.
Priestley, K., and D. McKenzie (2006), The thermal structure of the lithosphere from shear wave velocities, *Earth Planet. Sci. Lett.*, *244*, 285–301.
Priestley, K., and D. McKenzie (2013), The relationship between shear wave velocity, temperature, attenuation, and viscosity in the shallow part of the mantle, *Earth Planet. Sci. Lett.*, *381*, 78–91, doi:10.1016/j.epsl.2013.08.022.
Rajaram, M. (2007), Depth To Curie temperature, in *Encyclopedia of Geomagnetism and Paleomagnetism*, pp. 157–159, Springer, Netherlands.
Reading, A. M. (2007), The seismicity of the Antarctic plate, *Geol. Soc. Am. Spec. Pap.*, *425*, 285–298, doi:10.1130/2007.2425(18).
Ritzwoller, M. H., N. M. Shapiro, and S.-J. Zhong (2004), Cooling history of the Pacific lithosphere, *Earth Planet. Sci. Lett.*, *226*, 69–84, doi:10.1016/j.epsl.2004.07.032.
Röhm, A. H. E., R. Snieder, S. Goes, and J. Trampert (2000), Thermal structure of continental upper mantle inferred from *S*-wave velocity and surface heat flow, *Earth Planet. Sci. Lett.*, *181*, 395–407.
Rubin, K. H., and J. M. Sinton (2007), Inferences on mid-ocean ridge thermal and magmatic structure from MORB compositions, *Earth Planet. Sci. Lett.*, *260*, 257–276, doi:10.1016/j.epsl.2007.05.035.
Rudnick, L. R., W. F. McDonough, and R. J. O'Connel (1998), Thermal structure, thickness, and composition of continental lithosphere, *Chem. Geol.*, *145*, 395–411.
Rudnick, R. L., and D. M. Fountain (1995), Nature and composition of the continental crust: A lower crustal perspective, *Rev. Geophys.*, *33*, 267–309, doi:10.1029/95rg01302.
Schatz, J. F., and G. Simmons (1972), Thermal conductivity of Earth minerals at high temperatures, *J. Geophys. Res.*, *77*, 6966–6983, doi:10.1029/JB077i035p06966.
Schmerr, N. (2012), The Gutenberg Discontinuity: Melt at the lithosphere–asthenosphere boundary, *Science*, *335*, 1480–1483.
Schroeder, W. (1984), The empirical age–depth relation and depth anomalies in the Pacific Ocean Basin, *J. Geophys. Res.*, *89*, 9873–9883, doi:10.1029/JB089iB12p09873.
Schubert, G., D. L. Turcotte, and P. Olson (2001), *Mantle Convection in the Earth and Planets*, 956 pp., Cambridge Univ. Press, Cambridge, U. K.
Schuberth, B. S. A., H. P. Bunge, and J. Ritsema (2009), Tomographic filtering of high-resolution mantle circulation models: Can seismic heterogeneity be explained by temperature alone?, *Geochem. Geophys. Geosyst.*, *10*, Q05W03, doi:10.1029/2009GC002401.
Schutt, D. L., and C. E. Lesher (2006), Effects of melt depletion on the density and seismic velocity of garnet and spinel lherzolite, *J. Geophys. Res.*, *111*, B05401, doi:10.1029/2003JB002950.
Shapiro, N. M., and M. H. Ritzwoller (2004a), Thermodynamic constraints on seismic inversions, *Geophys. J. Int.*, *157*, 1175–1188, doi:10.1111/j.1365-246X.2004.02254.x.
Shapiro, N. M., and M. H. Ritzwoller (2004b), Inferring surface heat flux distributions guided by a global seismic model: Particular application to Antarctica, *Earth Planet. Sci. Lett.*, *223*, 213–224, doi:10.1016/j.epsl.2004.04.011.
Siddoway, C. S. (2008), Tectonics of the West Antarctic rift system: New light on the history and dynamics of distributed intracontinental extension, in *Antarctica: A Keystone in a Changing World —Online Proceedings of the 10th International Symposium on Antarctic Earth Sciences*, edited by A. K. Cooper et al., p. kp09, National Academies Press, Washington, D. C.
Siebert, L., and T. Simkin (2002), *Volcanoes of the World: An Illustrated Catalog of Holocene Volcanoes and their Eruptions*, Smithsonian Institution, Washington, D. C.
Siegert, M. J. (2000), Antarctic subglacial lakes, *Earth Sci. Rev.*, *50*, 29–50, doi:10.1016/S0012-8252(99)00068-9.
Siegert, M. J., and J. A. Dowdeswell (1996), Spatial variations in heat at the base of the Antarctic ice sheet from analysis of the thermal regime above subglacial lakes, *J. Glaciol.*, *42*, 501–509.
Siegert, M. J., S. Carter, I. Tabacco, S. Popov, and D. D. Blankenship (2005), A revised inventory of Antarctic subglacial lakes, *Antarct. Sci.*, *17*, 453–460, doi:10.1017/S0954102005002889.
Sobolev, S. V., H. Zeyen, G. Stoll, F. Werling, R. Altherr, and K. Fuchs (1996), Upper mantle temperatures from teleseismic tomography of French Massif Central including effects of composition, mineral reactions, anharmonicity, anelasticity and partial melt, *Earth Planet. Sci. Lett.*, *139*, 147–163.
Standish, J. J., H. J. B. Dick, P. J. Michael, W. G. Melson, and T. O'Hearn (2008), MORB generation beneath the ultraslow spreading Southwest Indian Ridge (9–25°E): Major element chemistry and the importance of process versus source, *Geochem. Geophys. Geosyst.*, *9*, Q05004, doi:10.1029/2008GC001959.
Stein, C. A., and S. Stein (1992), A model for the global variation in oceanic depth and heat flow with lithospheric age, *Nature*, *359*, 123–129.
Sutherland, R. (2008), The significance of Antarctica for studies of global geodynamics, in *Antarctica: A Keystone in a Changing World—Online Proceedings of the 10th International Symposium on Antarctic Earth Sciences*, edited by A. K. Cooper et al., p. kp10, National Academies Press, Washington, D. C.
Torsvik, T. H., C. Gaina, and T. F. Redfield (2008), Antarctica and global paleogeography: From Rodinia, through Gondwanaland and Pangea, to the birth of the Southern Ocean and the opening of gateways, in *Antarctica: A Keystone in a Changing World—Online Proceedings of the 10th International Symposium on Antarctic Earth Sciences*, edited by A. K. Cooper et al., p. kp11, National Academies Press, Washington, D. C.
Torsvik, T. H., B. Steinberger, M. Gurnis, and C. Gaina (2010), Plate tectonics and net lithosphere rotation over the past 150 My, *Earth Planet. Sci. Lett.*, *291*, 106–112, doi:10.1016/j.epsl.2009.12.055.
Vérard, C., K. Flores, and G. Stampfli (2012), Geodynamic reconstructions of the South America–Antarctica plate system, *J. Geodyn.*, *53*, 43–60, doi:10.1016/j.jog.2011.07.007.
Wang, Y., D. W. Forsyth, C. J. Rau, N. Carriero, B. Schmandt, J. B. Gaherty, and B. Savage (2013), Fossil slabs attached to unsubducted fragments of the Farallon plate, *Proc. Natl. Acad. Sci. U.S.A.*, *110*, 5342–5346.
Wasilewski, P. J., and M. A. Mayhew (1992), The Moho as a magnetic boundary revisited, *Geophys. Res. Lett.*, *19*, 2259–2262, doi:10.1029/92GL01997.
Wessel, P., and W. H. F. Smith (1991), Free software helps map and display data, *Eos Trans. AGU*, *72*, 441, doi:10.1029/90EO00319.
Whittington, A. G., A. M. Hofmeister, and P. I. Nabelek (2009), Temperature-dependent thermal diffusivity of the Earth's crust and implications for magmatism, *Nature*, *458*, 319–321, doi:10.1038/nature07818.

Winberry, J. P., and S. Anandakrishnan (2003), Seismicity and neotectonics of West Antarctica, *Geophys. Res. Lett.*, *30*(18), 1931, doi:10.1029/2003GL018001.

Wright, A., and M. Siegert (2012), A fourth inventory of Antarctic subglacial lakes, *Antarct. Sci.*, *24*, 659–664, doi:10.1017/S095410201200048X.

Xu, J., Z. Gao, J. Sun, and C. Song (2001), A preliminary study of the coupling relationship between basin and mountain in extensional environments: A case study of the Bohai Bay Basin and Taihang Mountains [in Chinese with English abstract], *Acta Geol. Sin.*, *75*, 165–174.

Xu, Y., T. J. Shankland, S. Linhardt, D. C. Rubie, F. Langenhorst, and K. Klasinski (2004), Thermal diffusivity and conductivity of olivine, wadsleyite and ringwoodite to 20 GPa and 1373 K, *Phys. Earth Planet. Inter.*, *143–144*, 321–336, doi:10.1016/j.pepi.2004.03.005.

Yang, Y., and D. W. Forsyth (2008), Attenuation in the upper mantle beneath Southern California: Physical state of the lithosphere and asthenosphere, *J. Geophys. Res.*, *113*, B03308, doi:10.1029/2007JB005118.